

# Fundamental limits on the rate of bacterial cell division

<sup>3</sup> **Nathan M. Belliveau<sup>†, 1</sup>, Griffin Chure<sup>†, 2, 3</sup>, Christina L. Hueschen<sup>4</sup>, Hernan G.  
<sup>4</sup> Garcia<sup>5</sup>, Jané Kondev<sup>6</sup>, Daniel S. Fisher<sup>7</sup>, Julie Theriot<sup>1, 8</sup>, Rob Phillips<sup>2, 9, \*</sup>**

\*For correspondence:

<sup>†</sup>These authors contributed equally to this work

<sup>5</sup> <sup>1</sup>Department of Biology, University of Washington, Seattle, WA, USA; <sup>2</sup>Division of  
<sup>6</sup> Biology and Biological Engineering, California Institute of Technology, Pasadena, CA,  
<sup>7</sup> USA; <sup>3</sup>Department of Applied Physics, California Institute of Technology, Pasadena, CA,  
<sup>8</sup> USA; <sup>4</sup>Department of Chemical Engineering, Stanford University, Stanford, CA, USA;  
<sup>9</sup> <sup>5</sup>Department of Molecular Cell Biology and Department of Physics, University of  
<sup>10</sup> California Berkeley, Berkeley, CA, USA; <sup>6</sup>Department of Physics, Brandeis University,  
<sup>11</sup> Waltham, MA, USA; <sup>7</sup>Department of Applied Physics, Stanford University, Stanford, CA,  
<sup>12</sup> USA; <sup>8</sup>Allen Institute for Cell Science, Seattle, WA, USA; <sup>9</sup>Department of Physics,  
<sup>13</sup> California Institute of Technology, Pasadena, CA, USA; \*Contributed equally

<sup>14</sup> 

---

<sup>15</sup> **Abstract** This will be written next

<sup>16</sup> 

---

## <sup>17</sup> Introduction

<sup>18</sup> The range of bacterial growth rates is enormously diverse. In natural environments, some micro-  
<sup>19</sup> bial organisms might double only once per year while in comfortable laboratory conditions, growth  
<sup>20</sup> can be rapid with several divisions per hour. This six order of magnitude difference illustrates the  
<sup>21</sup> intimate relationship between environmental conditions and the rates at which cells convert nu-  
<sup>22</sup> trients into new cellular material – a relationship that has remained a major topic of inquiry in  
<sup>23</sup> bacterial physiology for over a century (*Jun et al., 2018*). As was noted by Jacques Monod, “the  
<sup>24</sup> study of the growth of bacterial cultures does not constitute a specialized subject or branch of re-  
<sup>25</sup> search, it is the basic method of Microbiology.” Those words ring as true today as they did when  
<sup>26</sup> they were written 70 years ago. Indeed, the study of bacterial growth has undergone a molecular  
<sup>27</sup> resurgence since many of the key questions addressed by the pioneering efforts in the middle of  
<sup>28</sup> the last century can be revisited by examining them through the lens of the increasingly refined  
<sup>29</sup> molecular census that is available for bacteria such as the microbial workhorse *Escherichia coli*. Sev-  
<sup>30</sup> eral of the outstanding questions that can now be studied about bacterial growth include: what  
<sup>31</sup> sets the fastest time scale that bacteria can divide, and how is growth rate tied to the quality of the  
<sup>32</sup> carbon source. In this paper, we address these two questions from two distinct angles. First, as  
<sup>33</sup> a result of an array of high-quality proteome-wide measurements of the *E. coli* proteome under a  
<sup>34</sup> myriad of different growth conditions, we have a census that allows us to explore how the num-  
<sup>35</sup> ber of key molecular players change as a function of growth rate. This census provides a window  
<sup>36</sup> onto whether the processes they mediate such as molecular transport into the cells and molecular  
<sup>37</sup> synthesis within cells can run faster. Second, because of our understanding of the molecular path-  
<sup>38</sup> ways responsible for many of the steps in bacterial growth, we can also make order of magnitude  
<sup>39</sup> estimates to infer the copy numbers that would be needed to achieve a given growth rate. In this  
<sup>40</sup> paper, we pass back and forth between the analysis of a variety of different proteomic datasets and  
<sup>41</sup> order-of-magnitude estimations to determine possible molecular bottlenecks that limit bacterial

42 growth and to see how the growth rate varies in different carbon sources.

43 Specifically, we leverage a combination of *E. coli* proteomic data sets collected over the past  
 44 decade using either mass spectrometry (*Schmidt et al., 2016; Peebo et al., 2015; Valgepea et al.,  
 45 2013*) or ribosomal profiling (*Li et al., 2014*) across 31 unique growth conditions. Broadly speaking,  
 46 we entertain several classes of hypotheses as are illustrated in **Figure 1**. First, we consider potential  
 47 limits on the transport of nutrients into the cell. We address this hypothesis by performing an  
 48 order-of-magnitude estimate for how many carbon, phosphorous, and sulfur atoms are needed to  
 49 facilitate this requirement given a 5000 second division time. As a second hypothesis, we consider  
 50 the possibility that there exists a fundamental limit on how quickly the cell can generate ATP. We  
 51 approach this hypothesis from two angles, considering how many ATP synthase complexes must  
 52 be needed to churn out enough ATP to power protein translation followed by an estimation of  
 53 how many electron transport complexes must be present to maintain the proton motive force.  
 54 A third class of estimates considers the need to maintain the size and shape of the cell through  
 55 the construction of new lipids for the cell membranes as well as the glycan polymers which make  
 56 up the rigid peptidoglycan. Our final class of hypotheses centers on the synthesis of a variety of  
 57 biomolecules. Our focus is primarily on the stages of the central dogma as we estimate the number  
 58 of protein complexes needed for DNA replication, transcription, and protein translation.

59 In broad terms, we find that the majority of these estimates are in close agreement with the  
 60 experimental observations, with protein copy numbers apparently well-tuned for the task of cell  
 61 doubling. This allows us to systematically scratch off the hypotheses diagrammed in **Figure 1** as  
 62 setting possible speed limits. Ultimately, we find that protein translation (particularly the genera-  
 63 tion of new ribosomes) acts as 1) a rate limiting step for the *fastest* bacterial division, and 2) the  
 64 major determinant of bacterial growth across all nutrient conditions we have considered under  
 65 steady state, exponential growth. This perspective is in line with the linear correlation observed  
 66 between growth rate and ribosomal content (typically quantified through the ratio of RNA to pro-  
 67 tein) for fast growing cells (*Scott et al., 2010*), but suggests a more prominent role for ribosomes  
 68 in setting the doubling time across all conditions of nutrient limitation. Here we again leverage the  
 69 quantitative nature of this data set and present a quantitative model of the relationship between  
 70 the fraction of the proteome devoted to ribosomes and the speed limit of translation, revealing  
 71 a fundamental tradeoff between the translation capacity of the ribosome pool and the maximal  
 72 growth rate.

### 73 Uptake of Nutrients

74 In order to build new cellular mass, the molecular and elemental building blocks must be scav-  
 75 enged from the environment in different forms. Carbon, for example, is acquired via the transport  
 76 of carbohydrates and sugar alcohols with some carbon sources receiving preferential treatment  
 77 in their consumption (*Monod, 1947*). Phosphorus, sulfur, and nitrogen, on the other hand, are  
 78 harvested primarily in the forms of inorganic salts, namely phosphate, sulfate, and ammonia (*Jun  
 79 et al., 2018; Assentoft et al., 2016; Stasi et al., 2019; Antonenko et al., 1997; Rosenberg et al., 1977;  
 80 Willsky et al., 1973*). All of these compounds have different permeabilities across the cell mem-  
 81 brane and most require some energetic investment either via ATP hydrolysis or through the pro-  
 82 ton electrochemical gradient to bring the material across the hydrophobic cell membrane. Given  
 83 the diversity of biological transport mechanisms and the vast number of inputs needed to build a  
 84 cell, we begin by considering transport of some of the most important cellular ingredients: carbon,  
 85 nitrogen, oxygen, hydrogen, phosphorus, and sulfur.

86 The elemental composition of *E. coli* has received much quantitative attention over the past  
 87 half century (*Neidhardt et al., 1991; Taymaz-Nikerel et al., 2010; Heldal et al., 1985; Bauer and  
 88 Ziv, 1976*), providing us with a starting point for estimating the copy numbers of various trans-  
 89 porters. While there is some variability in the exact elemental percentages (with different uncer-  
 90 tainties), we can estimate that the dry mass of a typical *E. coli* cell is  $\approx$  45% carbon (BNID: 100649,  
 91 *Milo et al. (2010)*),  $\approx$  15% nitrogen (BNID: 106666, *Milo et al. (2010)*),  $\approx$  3% phosphorus (BNID:

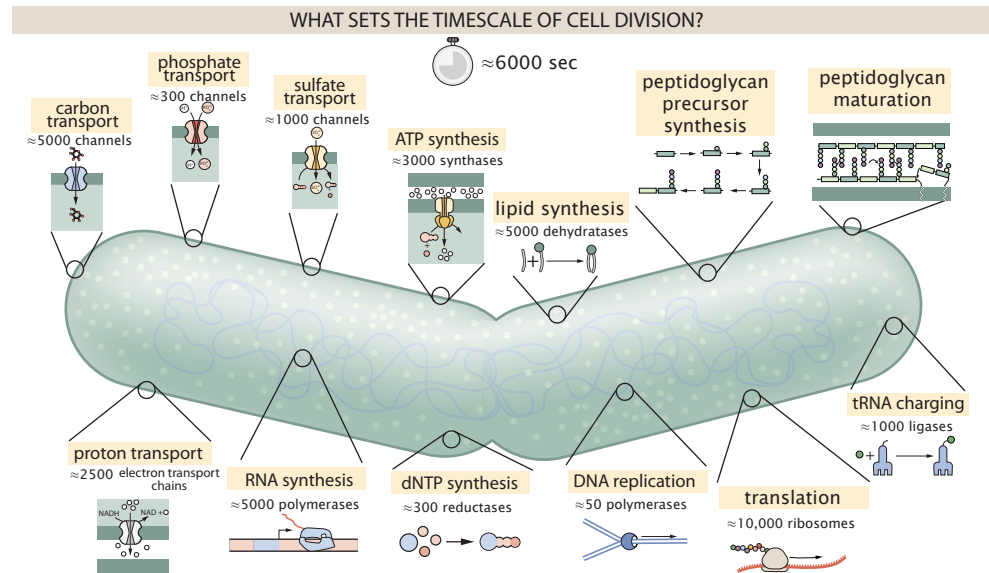


**Figure 1. Transport and synthesis processes necessary for cell division.** We consider an array of processes necessary for a cell to double its molecular components. Such processes include the transport of carbon across the cell membrane, the production of ATP, and fundamental processes of the central dogma namely RNA, DNA, and protein synthesis. A schematic of each synthetic or transport category is shown with an approximate measure of the complex abundance at a growth rate of 0.5 per hour. In this work, we consider a standard bacterial division time of  $\approx 5000$  sec.

92 100653, *Milo et al. (2010)*), and 1% sulfur (BNID: 100655, *Milo et al. (2010)*). In the coming para-  
 93 graphs, we will engage in a dialogue between back-of-the-envelope estimates for the numbers of  
 94 transporters needed to facilitate these chemical stoichiometries and the experimental proteomic  
 95 measurements of the biological reality. Such an approach provides the opportunity to test if our  
 96 biological knowledge is sufficient to understand the scale at which these complexes are produced.  
 97 Specifically, we will make these estimates considering a modest doubling time of 5000 s, a growth  
 98 rate of  $\approx 0.5 \text{ hr}^{-1}$ , the range in which the majority of the experimental measurements reside.

### 99 Nitrogen Transport

100 Before we begin our back-of-the-envelope estimations, we must address which elemental sources  
 101 must require proteinaceous transport, meaning that the cell cannot acquire appreciable amounts  
 102 simply via diffusion from the membrane. The permeability of the lipid membrane to a large num-  
 103 ber of solutes has been extensively characterized over the past century. Large, polar molecular  
 104 species (such as various sugar molecules, sulfate, and phosphate) have low permeabilities while  
 105 small, non-polar compounds (such as oxygen, carbon dioxide, and ammonia) can readily diffuse  
 106 across the membrane. Ammonia, a primary source of nitrogen in typical laboratory conditions,  
 107 has a permeability on par with water ( $\approx 10^5 \text{ nm/s}$ , BNID:110824 *Milo et al. (2010)*). In particularly  
 108 nitrogen-poor conditions, *E. coli* expresses a transporter (AmtB) which appears to aid in nitrogen  
 109 assimilation, though the mechanism and kinetic details of transport is still a matter of debate (*van*  
 110 *Heeswijk et al., 2013; Khademi et al., 2004*). Beyond ammonia, another plentiful source of nitrogen  
 111 come in the form of glutamate, which has its own complex metabolism and scavenging pathways.  
 112 However, nitrogen is plentiful in the growth conditions examined in this work, permitting us to ne-  
 113 glect nitrogen transport as a potential rate limiting process in cell division in typical experimental  
 114 conditions. We direct the reader to the supplemental information for a more in-depth discussion of  
 115 permeabilities and a series of calculations revealing that active nitrogen transport can be neglected  
 116 for the purposes of this article.

**117 Carbon Transport**

**118** We begin our estimations with the most abundant element in *E. coli* by mass, carbon. Using  $\approx 0.3$   
**119** pg as the typical *E. coli* dry mass (BNID: 103904, *Milo et al. (2010)*), we estimate that  $\approx 10^{10}$  carbon  
**120** atoms must be brought into the cell in order to double all of the carbon-containing molecules (*Fig-*  
**121** *ure 2(A, top)*). Typical laboratory growth conditions, such as those explored in the aforementioned  
**122** proteomic data sets, provide carbon as a single class of sugar such as glucose, galactose, or xylose  
**123** to name a few. *E. coli* has evolved myriad mechanisms by which these sugars can be transported  
**124** across the cell membrane. One such mechanism of transport is via the PTS system which is a  
**125** highly modular system capable of transporting a diverse range of sugars (*Escalante et al., 2012*).  
**126** The glucose-specific component of this system transports  $\approx 200$  glucose molecules per second per  
**127** transporter (BNID: 114686, *Milo et al. (2010)*). Making the assumption that this is a typical sugar  
**128** transport rate, coupled with the need to transport  $10^{10}$  carbon atoms, we arrive at the conclusion  
**129** that on the order of 1,000 transporters must be expressed in order to bring in enough carbon  
**130** atoms to divide in 5000 s, diagrammed in the top panel of *Figure 2(A)*. This estimate, along with  
**131** the observed average number of the PTS system carbohydrate transporters present in the pro-  
**132** teomic data sets (*Schmidt et al., 2016; Peebo et al., 2015; Valgepea et al., 2013; Li et al., 2014*), is  
**133** shown in *Figure 2(A)*. While we estimate 1500 transporters are needed with a 5000 s division time,  
**134** we can abstract this calculation to consider any particular growth rate given knowledge of the cell  
**135** density and volume as a function of growth rate and direct the reader to the SI for more informa-  
**136** tion. As revealed in *Figure 2(A)*, experimental measurements exceed the estimate by several fold,  
**137** illustrating that transport of carbon in to the cell is not rate limiting for cell division.

**138** The estimate presented in *Figure 2(A)* neglects any specifics of the regulation of carbon trans-  
**139** port system and presents a data-averaged view of how many carbohydrate transporters are present  
**140** on average. Using the diverse array of growth conditions explored in the proteomic data sets, we  
**141** can explore how individual carbon transport systems depend on the population growth rate. In  
**142** *Figure 2(B)*, we show the total number of carbohydrate transporters specific to different carbon  
**143** sources. A striking observation, shown in the top-left plot of *Figure 2(B)*, is the constancy in the  
**144** expression of the glucose-specific transport systems. Additionally, we note that the total number  
**145** of glucose-specific transporters is tightly distributed  $\approx 10^4$  per cell, the approximate number of  
**146** transporters needed to sustain rapid growth of several divisions per hour, as indicated by the grey  
**147** shaded line. This illustrates that *E. coli* maintains a substantial number of complexes present for  
**148** transporting glucose which is known to be the preferential carbon source (*Monod, 1947; Liu et al.,*  
**149** *2005; Aidelberg et al., 2014*).

**150** It is now understood that a large number of metabolic operons are regulated with dual-input  
**151** logic gates that are only expressed when glucose concentrations are low (mediated by cyclic-AMP  
**152** receptor protein CRP) and the concentration of other carbon sources are elevated (*Gama-Castro*  
**153** *et al., 2016; Zhang et al., 2014b*). A famed example of such dual-input regulatory logic is in the regu-  
**154** lation of the *lac* operon which is only natively activated in the absence of glucose and the presence  
**155** of allolactose, an intermediate in lactose metabolism (*Jacob and Monod, 1961*), though we now  
**156** know of many other such examples (*Ireland et al., 2020; Gama-Castro et al., 2016; Belliveau et al.,*  
**157** *2018*). This illustrates that once glucose is depleted from the environment, cells have a means to  
**158** dramatically increase the abundance of the specific transporter needed to digest the next sugar  
**159** that is present. Several examples of induced expression of specific carbon-source transporters are  
**160** shown in *Figure 2(B)*. Points colored in red (labeled by red text-boxes) correspond to growth condi-  
**161** tions in which the specific carbon source (glycerol, xylose, or fructose) is present. These plots show  
**162** that, in the absence of the particular carbon source, expression of the transporters is maintained  
**163** on the order of  $\sim 10^2$  per cell. However, when induced, the transporters become highly-expressed  
**164** and fall close to the predicted number of transporters needed to facilitate growth on that sub-  
**165** strate alone, shown as a transparent grey line. Together, this generic estimation and the specific  
**166** examples of induced expression suggest that transport of carbon across the cell membrane, while

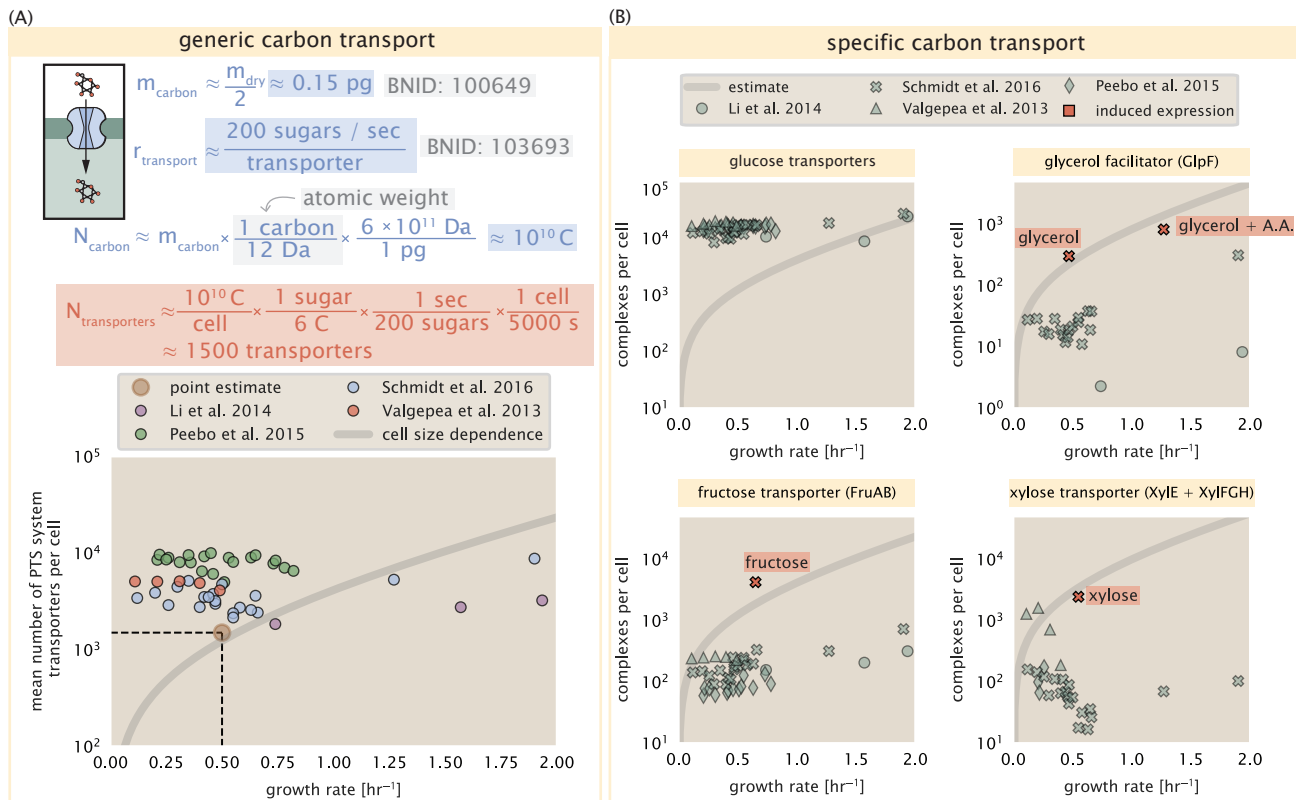


**Figure 2. The abundance of carbon transport systems across growth rates.** (A) A simple estimate for the minimum number of generic carbohydrate transport systems (top) assumes  $\approx 10^{10}$  C are needed to complete division, each transported sugar contains  $\approx 6$  C, and each transporter conducts sugar molecules at a rate of  $\approx 200$  per second. Bottom plot shows the estimated number of transporters needed at a growth rate of  $\approx 0.5$  per hr (light-brown point and dashed lines). Colored points correspond to the mean number of PTS system sugar transporters (complexes annotated with the Gene Ontology term GO:0009401) for different growth conditions across different published datasets. (B) The abundance of various specific carbon transport systems plotted as a function of the population growth rate. Red points and red-highlighted text indicate conditions in which the only source of carbon in the growth medium induces expression of the transport system. Grey line in (A) and (B) represents the estimated number of transporters per cell at a continuum of growth rates.

167 critical for growth, is not the rate-limiting step of cell division.

### 168 **Phosphorus and Sulfur Transport**

169 We now turn our attention towards other essential elements, namely phosphorus and sulfur. Phos-  
 170 phorus is critical to the cellular energy economy in the form of high-energy phosphodiester bonds  
 171 making up DNA, RNA, and the NTP energy pool as well as playing a critical role in the post-translational  
 172 modification of proteins and defining the polar-heads of lipids. In total, phosphorus makes up  
 173 ≈3% of the cellular dry mass which in typical experimental conditions is in the form of inorganic  
 174 phosphate. The cell membrane has remarkably low permeability to this highly-charged and critical  
 175 molecule, therefore requiring the expression of active transport systems. In *E. coli*, the proton elec-  
 176 trochemical gradient across the inner membrane is leveraged to transport inorganic phosphate  
 177 into the cell (*Rosenberg et al., 1977*). Proton-solute symporters are widespread in *E. coli* (*Ramos*  
 178 and *Kaback, 1977; Booth et al., 1979*) and can have rapid transport rates of 50 to 100 molecules  
 179 per second for sugars and other solutes (BNID: 103159; 111777, *Milo et al. (2010)*). As a more  
 180 extreme example, the proton transporters in the F<sub>1</sub>-F<sub>0</sub> ATP synthase, which leverage the proton  
 181 electrochemical gradient for rotational motion, can shuttle protons across the membrane at a rate  
 182 of ≈ 1000 per second (BNID: 104890; 103390, *(Milo et al., 2010)*). In *E. coli* the PitA phosphate trans-  
 183 port system has been shown to be very tightly coupled with the proton electrochemical gradient  
 184 with a 1:1 proton:phosphate stoichiometric ratio (*Harris et al., 2001; Feist et al., 2007*). Taking the  
 185 geometric mean of the aforementioned estimates gives a plausible rate of phosphate transport  
 186 on the order of 300 per second. Illustrated in *Figure 3(A)*, we can estimate that ≈ 150 phosphate  
 187 transporters are necessary to maintain an ≈ 3% dry mass with a 5000 s division time. This estimate  
 188 is again satisfied when we examine the observed copy numbers of PitA in proteomic data sets (plot  
 189 in *Figure 3(A)*). While our estimate is very much in line with the observed numbers, we emphasize  
 190 that this is likely a slight overestimate of the number of transporters needed as there are other  
 191 phosphorous scavenging systems, such as the ATP-dependent phosphate transporter Pst system  
 192 which we have neglected.

193 Satisfied that there are a sufficient number of phosphate transporters present in the cell, we  
 194 now turn to sulfur transport as another potentially rate limiting process. Similar to phosphate,  
 195 sulfate is highly-charged and not particularly membrane permeable, requiring active transport.  
 196 While there exists a H+/sulfate symporter in *E. coli*, it is in relatively low abundance and is not well  
 197 characterized (*Zhang et al., 2014a*). Sulfate is predominantly acquired via the ATP-dependent ABC  
 198 transporter CysUWA system which also plays an important role in selenium transport (*Sekowska*  
 199 *et al., 2000; Sirko et al., 1995*). While specific kinetic details of this transport system are not readily  
 200 available, generic ATP transport systems in prokaryotes transport on the order of 1 to 10 molecules  
 201 per second (BNID: 109035, *Milo et al. (2010)*). Combining this generic transport rate, measurement  
 202 of sulfur comprising 1% of dry mass, and a 5000 second division time yields an estimate of ≈ 1000  
 203 CysUWA complexes per cell (*Figure 3(B)*). Once again, this estimate is in notable agreement with  
 204 proteomic data sets, suggesting that there are sufficient transporters present to acquire the nec-  
 205 essary sulfur. In a similar spirit of our estimate of phosphorus transport, we emphasize that this is  
 206 likely an overestimate of the number of necessary transporters as we have neglected other sulfur  
 207 scavenging systems that are in lower abundance.

### 208 **Limits on Transporter Expression**

209 So which, if any, of these processes may be rate limiting for growth? As suggested by *Figure 2*  
 210 (B), induced expression can lead to an order-of-magnitude (or more) increase in the amount of  
 211 transporters needed to facilitate transport. Thus, if acquisition of nutrients was the limiting state  
 212 in cell division, could expression simply be increased to accommodate faster growth? A way to  
 213 approach this question is to compute the amount of space in the bacterial membrane that could  
 214 be occupied by nutrient transporters. Considering a rule-of-thumb for the surface area of *E. coli* of  
 215 about 6  $\mu\text{m}^2$  (BNID: 101792, *Milo et al. (2010)*), we expect an areal density for 1000 transporters to

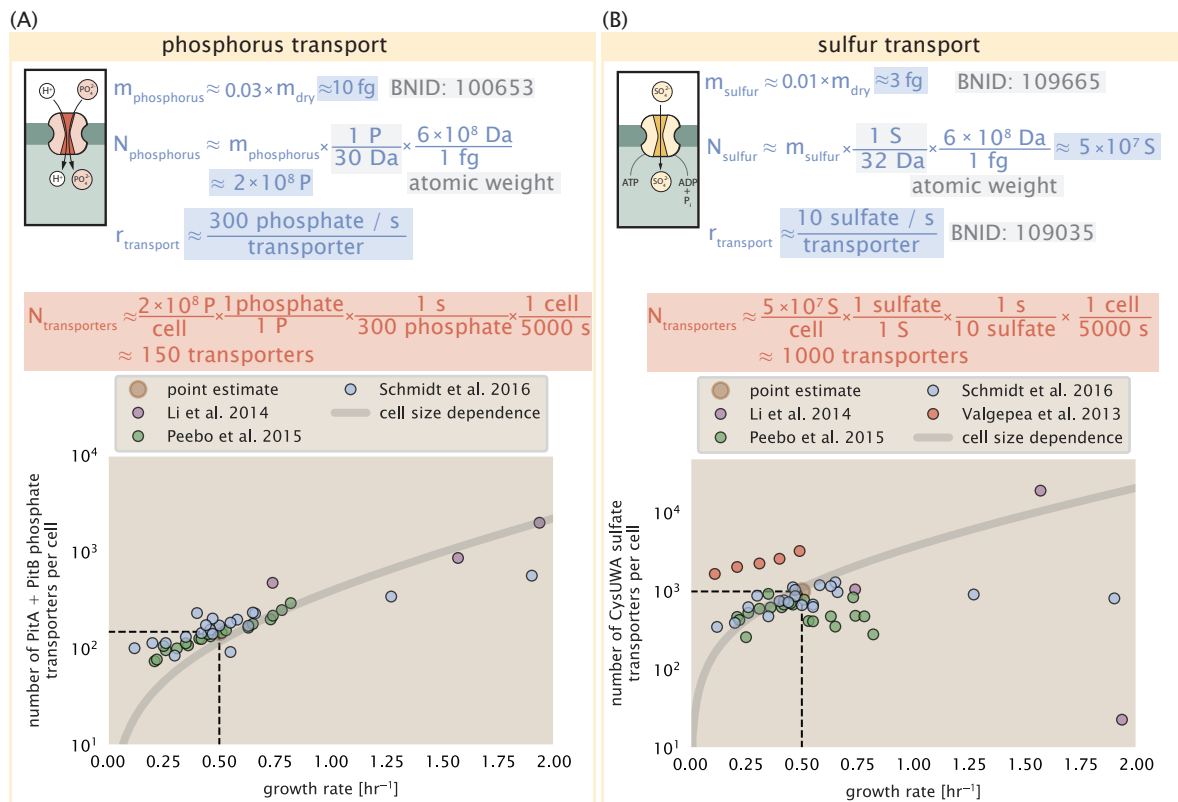


**Figure 3. Estimates and measurements of phosphate and sulfate transport systems as a function of growth rate.** (A) Estimate for the number of PitA phosphate transport systems needed to maintain a 3% phosphorus *E. coli* dry mass. Points in plot correspond to the total number of PitA transporters per cell. (B) Estimate of the number of CysUWA complexes necessary to maintain a 1% sulfur *E. coli* dry mass. Points in plot correspond to average number of CysUWA transporter complexes that can be formed given the transporter stoichiometry [CysA]<sub>2</sub>[CysU][CysW][Sbp/CysP]. Grey line in (A) and (B) represents the estimated number of transporters per cell at a continuum of growth rates.

216 be approximately 200 transporters/ $\mu\text{m}^2$ . For a typical transporter occupying about 50 nm $^2$ /dimer,  
 217 this amounts to about only 1 percent of the total inner membrane (*Szenk et al., 2017*). In addition,  
 218 bacterial cell membranes typically have densities of 10<sup>5</sup> proteins/ $\mu\text{m}^2$  (*Phillips, 2018*), implying that  
 219 the cell could accommodate more transporters of a variety of species if it were rate limiting. As we  
 220 will see in the next section, however, occupancy of the membrane can impose other limits on the  
 221 rate of energy production.

## 222 Energy Production

223 While the transport of nutrients is required to build new cell mass, the metabolic pathways both  
 224 consume and generate energy in the form of NTPs. The high-energy phosphodiester bonds of  
 225 (primarily) ATP power a variety of cellular processes that drive biological systems away from ther-  
 226 modynamic equilibrium. The next set of processes we hypothesize might control the rate of cell  
 227 division considers the energy budget of a dividing cell in terms of the synthesis of ATP from ADP  
 228 and inorganic phosphate as well as maintenance of the electrochemical proton gradient which  
 229 powers it.

## 230 ATP Synthesis

231 Hydrolysis of the terminal phosphodiester bond of ATP forming ADP and an inorganic phosphate is  
 232 a kinetic driving force in a wide array of biochemical reactions. One such reaction is the formation  
 233 of peptide bonds during translation which requires  $\approx$  2 ATPs for the charging of an amino acid  
 234 to the tRNA and  $\approx$  2 ATP equivalents for the formation of the peptide bond between amino acids.  
 235 Considering the ATP costs associated with error correction and post-translational modifications  
 236 of proteins, we can make the approximation that each peptide bond has a net cost of  $\approx$  5 ATP  
 237 (BNID: 107782, *Milo et al. (2010)*). In total, the energetic costs of peptide bond formation consume  
 238  $\approx$  80% of the cells ATP budget (BNID: 107782; 106158; 101637; 111918, *Milo et al. (2010); Lynch*  
 239 *and Marinov (2015); Stouthamer (1973)*). The pool of ATP is produced by the F<sub>1</sub>-F<sub>0</sub> ATP synthase  
 240 – a membrane-bound rotary motor which under ideal conditions can yield  $\approx$  300 ATP per second  
 241 (BNID: 114701; *Milo et al. (2010); Weber and Senior (2003)*).

242 To estimate the total number of ATP equivalents consumed during a cell cycle, we will make  
 243 the approximation that there are  $\approx$  3  $\times$  10<sup>6</sup> proteins per cell with an average protein length of  $\approx$  300  
 244 peptide bonds (BNID: 115702; 108986; 104877, *Milo et al. (2010)*). Taking these values together,  
 245 we estimate that the typical *E. coli* cell consumes  $\approx$  5  $\times$  10<sup>9</sup> ATP per cell cycle on protein synthesis  
 246 alone and  $\approx$  6  $\times$  10<sup>9</sup> ATP in total. Assuming that the ATP synthases are operating at their fastest  
 247 possible rate,  $\approx$  3000 ATP synthases are needed to keep up with the energy demands of the cell.  
 248 This estimate and a comparison with the data are shown in *Figure 4* (A). Despite our assumption  
 249 of maximal ATP production rate per synthase and approximation of all NTP consuming reactions  
 250 being the same as ATP, we find that an estimate of a few thousand complete synthases per cell  
 251 to agree well with the experimental data. Much as we did for the estimates of transporter copy  
 252 number in the previous section, we can generalize this estimation to consider a continuum of  
 253 growth rates rather than a point estimate of 5000 s, indicated by the gray lines in *Figure 4*, and find  
 254 that this approach adequately describes the observed growth rate dependence.

255 If the direct production of ATP was a rate limiting step for growth, could the cell simply express  
 256 more ATP synthase complexes? This requires us to consider several features of cellular physiology,  
 257 namely the physical space on the inner membrane as well as the ability to maintain the proton  
 258 chemical gradient leveraged by the synthase to drive ATP production out of equilibrium.

## 259 Generating the Proton Electrochemical Gradient

260 In order to produce ATP, the F<sub>1</sub>-F<sub>0</sub> ATP synthase itself must consume energy. Rather than burning  
 261 through its own product, this intricate macromolecular machine has evolved to exploit the elec-  
 262 trochemical potential established across the inner membrane through cellular respiration. This  
 263 electrochemical gradient is manifest by the pumping of protons into the intermembrane space via

264 the electron transport chains as they reduce NADH. In *E. coli*, this potential difference is  $\approx -200$  mV  
 265 (BNID: 102120, *Milo et al. (2010)*). A simple estimate of the inner membrane as a capacitor with a  
 266 working voltage of -200 mV (as performed in the Supplemental Information) reveals that  $\approx 2 \times 10^4$   
 267 protons must be present in the intermembrane space.

268 However, the constant rotation of the ATP synthases would rapidly abolish this potential difference if it were not being actively maintained. To undergo a complete rotation (and produce a  
 269 single ATP), the F<sub>1</sub>-F<sub>0</sub> ATP synthase must shuttle  $\approx 4$  protons across the membrane into the cytosol  
 270 (BNID: 103390, *Milo et al. (2010)*). With  $\approx 3000$  ATP synthases each generating 300 ATP per second,  
 271 the  $2 \times 10^4$  protons establishing the 200 mV potential would be consumed in only a few milliseconds.  
 272 This brings us to our next estimate: how many electron transport complexes are needed to support the consumption rate of the ATP synthases?

273 The electrochemistry of the electron transport complexes of *E. coli* have been the subject of  
 274 intense biochemical and biophysical study over the past half century (*Ingledew and Poole, 1984;*  
*Khademian and Imlay, 2017; Cox et al., 1970; Henkel et al., 2014*). A recent work (*Szenk et al., 2017*) examined the respiratory capacity of the *E. coli* electron transport complexes using structural and biochemical data, revealing that each electron transport chain rapidly pumps protons into the intermembrane space at a clip of  $\approx 1500$  protons per second (BIND: 114704; 114687, *Milo et al. (2010)*). Using our estimate of the number of ATP synthases required per cell (*Figure 4(A)*), coupled with these recent measurements, we estimate that  $\approx 1000$  electron transport complexes would be necessary to facilitate the  $\approx 4 \times 10^6$  protons per second diet of the cellular ATP synthases. This estimate (along with a generalization to the entire range of observed growth rates) is in agreement with the number of complexes identified in the proteomic datasets (plot in *Figure 4(B)*). This suggests that every ATP synthase must be accompanied by  $\approx 1$  functional electron transport chain. Again, if this were a rate limiting process for bacterial growth, one must conclude that it is not possible for the cell to simply increase the production of both the number of electron transport chain complexes as well as ATP synthases. As both of these components only function bound to the inner membrane, we now turn our attention towards the available space in the membrane as well as surface-area-to-volume constraints.

## 292 Energy Production in a Crowded Membrane.

293 For each protein considered so far, the data shows that in general their numbers increase with  
 294 growth rate. This is in part a consequence of the increase in cell length and width at that is common  
 295 to many rod-shaped bacteria at faster growth rates (*Ojikic et al., 2019; Harris and Theriot, 2018*).  
 296 For the particular case of *E. coli*, the total cellular protein and cell size increase logarithmically  
 297 with growth rate (*Schaechter et al., 1958; Si et al., 2017*). Indeed, this is one reason why we have  
 298 considered only a single, common growth condition across all our estimates so far. Such a scaling  
 299 will require that the total number of proteins and net demand on resources also grow in proportion  
 300 to the increase in cell size divided by the cell's doubling time. Recall however that each transport  
 301 process, as well as the ATP production via respiration, is performed at the bacterial membrane.  
 302 This means that their maximum productivity can only increase in proportion to the cell's surface  
 303 area divided by the cell doubling time. This difference in scaling would vary in proportion to the  
 304 surface area-to-volume (S/V) ratio.

305 While we found that there was more than sufficient membrane real estate for carbon intake in  
 306 our earlier estimate, the total number of ATP synthases and electron chain transport complexes  
 307 both exhibit a clear increase in copy number with growth rate, reaching in excess of  $10^4$  copies per  
 308 cell (*Figure 4*). Here we consider the consequences of this S/V ratio scaling in more detail.

309 In our estimate of ATP production above we found that a cell demands about  $6 \times 10^9$  ATP or  $10^6$   
 310 ATP/s. With a cell volume of roughly 1 fL, this corresponds to about  $2 \times 10^{10}$  ATP per fL of cell volume,  
 311 in line with previous estimates (*Stouthamer and Bettenhausen, 1977; Szenk et al., 2017*). In *Figure 5* (A) we plot this ATP demand as a function of the S/V ratio in green, where we have considered  
 312 a range of cell shapes from spherical to rod-shaped with an aspect ratio (length/width) equal to 4

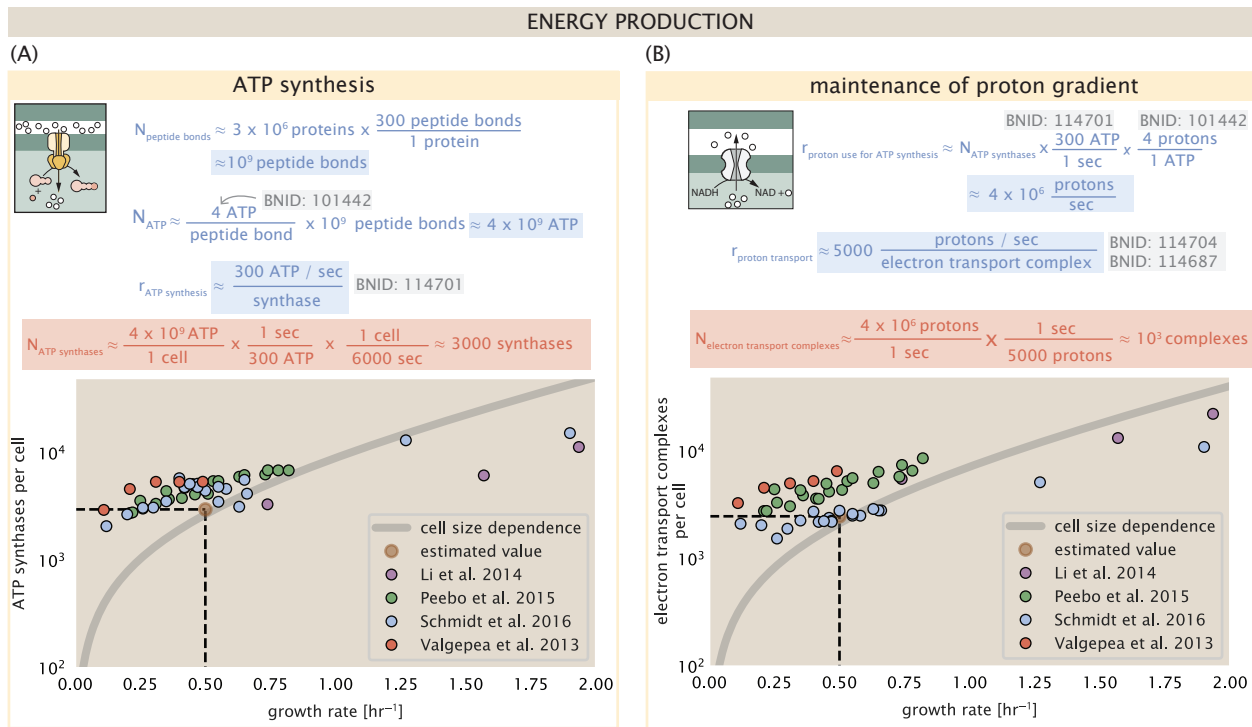


**Figure 4. The abundance of F<sub>1</sub>-F<sub>0</sub> ATP synthases and electron transport chain complexes as a function of growth rate.** (A) Estimate of the number of F<sub>1</sub>-F<sub>0</sub> ATP synthase complexes needed to accommodate peptide bond formation and other NTP dependent processes. Points in plot correspond to the mean number of complete F<sub>1</sub>-F<sub>0</sub> ATP synthase complexes that can be formed given proteomic measurements and the subunit stoichiometry [AtpE]<sub>10</sub>[AtpF]<sub>2</sub>[AtpB][AtpC][AtpH][AtpA]<sub>3</sub>[AtpG][AtpD]<sub>3</sub>. (B) Estimate of the number of electron transport chain complexes needed to maintain a membrane potential of -200 mV given estimate of number of F<sub>1</sub>-F<sub>0</sub> ATP synthases from (A). Points in plot correspond to the average number of complexes identified as being involved in aerobic respiration by the Gene Ontology identifier GO:0019646 that could be formed given proteomic observations. These complexes include cytochromes *bd1* ([CydA][CydB][CydX][CydH]), *bdII* ([AppC][AppB]), *bo3*, ([CyoD][CyoA][CyoB][CyoC]) and NADH:quinone oxioreductase I ([NuoA][NuoH][NuoJ][NuoK][NuoL][NuoM][NuoN][NuoB][NuoC][NuoE][NuoF][NuoG][NuoI]) and II ([Ndh]). Grey lines in both (A) and (B) correspond to the estimate procedure described, but applied to a continuum of growth rates. We direct the reader to the Supporting Information for a more thorough description of this approach.

**314** (See appendix for calculations of cell volume and surface area). In order to consider the maximum  
**315** power that could be produced, we consider the amount of ATP that can be generated by a membrane  
**316** filled with ATP synthase and electron transport complexes, which provides a maximal production  
**317** of about 3 ATP / (nm<sup>2</sup>·s) (*Szenk et al., 2017*). This is shown in blue in **Figure 5(A)**, which shows that  
**318** at least for the growth rates observed, the energy demand is roughly an order of magnitude less.

**319** Interestingly, *Szenk et al. (2017)* also found that ATP production by respiration is less efficient  
**320** than by fermentation per membrane area occupied due to the additional proteins of the electron  
**321** transport chain. This suggests that even under anaerobic growth, there will be sufficient mem-  
**322** brane space for ATP production in general.

**323** While this serves to highlight the diminishing capacity to provide resources to grow if the cell  
**324** increases in size (and its S/V decreases), the blue region in **Figure 5(A)** represents a somewhat  
**325** unachievable limit since the inner membrane must also include other proteins such as those re-  
**326** quired for lipid and membrane synthesis. To gain insight, we used the proteomic data to look at  
**327** the distribution of proteins on the inner membrane. Here we use Gene Ontology (GO) annotations  
**328** (*Ashburner et al., 2000; The Gene Ontology Consortium, 2018*) to identify all proteins embedded  
**329** or peripheral to the inner membrane (GO term: 0005886). Those associated but not membrane-  
**330** bound include proteins like MreB and FtsZ, that traverse the inner membrane by treadmilling and  
**331** must nonetheless be considered as a vital component occupying space on the membrane. In **Fig-  
**332** ure 5(B), we find that the total protein mass per μm<sup>2</sup> is relatively constant with growth rate. Inter-  
**333** estingly, when we consider the distribution of proteins grouped by their Clusters of Orthologous  
**334** Groups (COG) (*Tatusov et al., 2000*), the relative abundance for those in metabolism (including ATP  
**335** synthesis via respiration) is also relatively constant.**

### **336 Function of the Central Dogma**

**337** Up to this point, we have considered a variety of transport and biosynthetic processes that are  
**338** critical to acquiring and generating new cell mass. While there are of course many other metabolic  
**339** processes we could consider and perform estimates of (such as the components of fermentative  
**340** versus aerobic respiration), we now turn our focus to some of the most central processes which  
**341** *must* be undertaken irrespective of the growth conditions – the processes of the central dogma.

### **342 DNA**

**343** Most bacteria (including *E. coli*) harbor a single, circular chromosome and can have extra-chromosomal  
**344** plasmids up to ~ 100 kbp in length. We will focus our quantitative thinking solely on the chromo-  
**345** some of *E. coli* which harbors ≈ 5000 genes and ≈ 5 × 10<sup>6</sup> base pairs. To successfully divide and  
**346** produce viable progeny, this chromosome must be faithfully replicated and segregated into each  
**347** nascent cell. We again rely on the near century of literature in molecular biology to provide some  
**348** insight on the rates and mechanics of the replicative feat as well as the production of the required  
**349** starting materials, dNTPs.

### **350 dNTP synthesis**

**351** We begin our exploration DNA replication by examining the production of the deoxyribonucleotide  
**352** triphosphates (dNTPs). The four major dNTPs (dATP, dTTP, dCTP, and dGTP) are synthesized *de*  
**353** *novo* in separate pathways, requiring different building blocks. However, a critical step present in  
**354** all dNTP synthesis pathways is the conversion from ribonucleotide to deoxyribonucleotide via the  
**355** removal of the 3' hydroxyl group of the ribose ring (*Rudd et al., 2016*). This reaction is mediated  
**356** by a class of enzymes termed ribonucleotide reductases, of which *E. coli* possesses two aerobically  
**357** active complexes (termed I and II) and a single anaerobically active enzyme. Due to their peculiar  
**358** formation of a radical intermediate, these enzymes have received much biochemical, kinetic, and  
**359** structural characterization. One such work (*Ge et al., 2003*) performed a detailed *in vitro* measure-  
**360** ment of the steady-state kinetic rates of these complexes, revealing a turnover rate of ≈ 10 dNTP  
**361** per second.

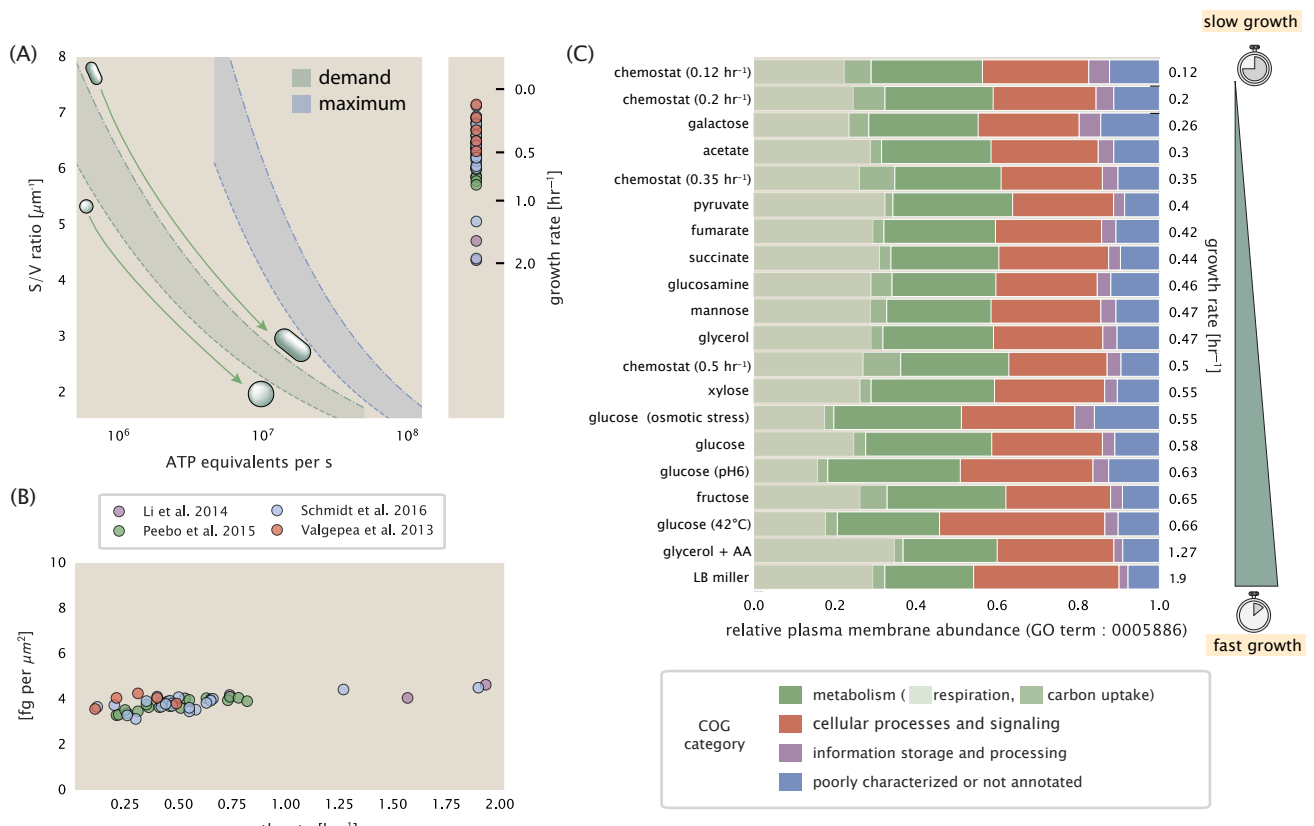


**Figure 5. Influence of cell size and S/V ratio on ATP production and inner membrane composition.** (A) Scaling of ATP demand and maximum ATP production as a function of S/V ratio. Cell volumes of 0.5 fL to 50 fL were considered, with the dashed (—) line corresponding to a sphere and the dash-dot line (---) reflecting a rod-shaped bacterium like *E. coli* with a typical aspect ratio (length / width) of 0.4. Approximately 50% of the bacterial inner membrane is assumed to be protein, with the remainder lipid. (B) Total protein mass calculated for proteins with inner membrane annotation (GO term: 0005886). (C) Relative protein abundances by mass based on COG annotation. Metabolic proteins are further separated into respiration ( $F_1$ - $F_0$  ATP synthase, NADH dehydrogenase I, succinate:quinone oxidoreductase, cytochrome bo<sub>3</sub> ubiquinol oxidase, cytochrome bd-I ubiquinol oxidase) and carbohydrate transport (GO term: GO:0008643). Note that the elongation factor EF-Tu can also associate with the inner membrane, but was excluded in this analysis due to its high relative abundance (roughly identical to the total mass shown in part (B)).

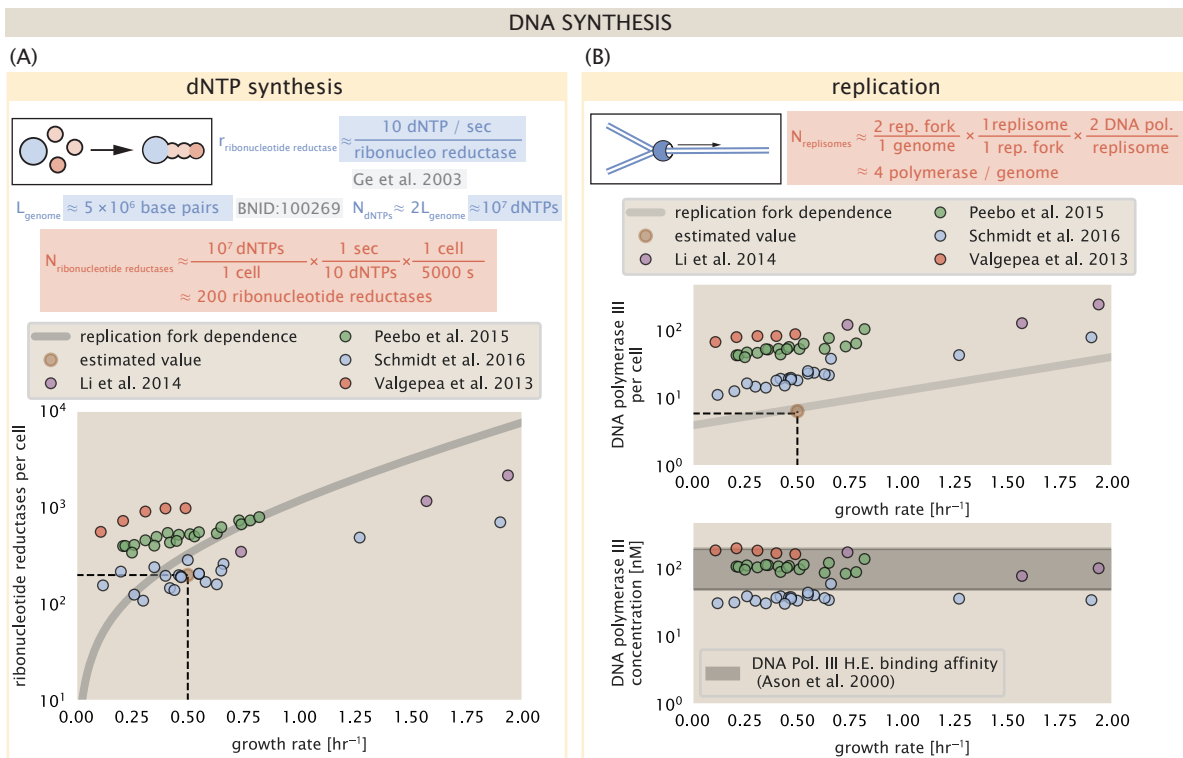


**Figure 6. Complex abundance estimates for dNTP synthesis and DNA replication.** (A) Estimate of the number of ribonucleotide reductase enzymes needed to facilitate the synthesis of  $\approx 10^7$  dNTPs over the course of a 6000 second generation time. Points in the plot correspond to the total number of ribonucleotide reductase I ( $[\text{NrdA}]_2[\text{NrdB}]_2$ ) and ribonucleotide reductase II ( $[\text{NrdE}]_2[\text{NrdF}]_2$ ) complexes. (B) An estimate for the minimum number of DNA polymerase holoenzyme complexes needed to facilitate replication of a single genome. Points in the top plot correspond to the total number of DNA polymerase III holoenzyme complexes ( $[\text{DnaE}]_3[\text{DnaQ}]_3[\text{Hole}]_3[\text{DnaX}]_5[\text{HolB}]_5[\text{HolA}]_5[\text{DnaN}]_4[\text{HolC}]_4[\text{Hold}]_4$ ) per cell. Bottom plot shows the effective concentration of DNA polymerase III holoenzyme given cell volumes calculated from the growth rate as in *Si et al. (2019)* (See Appendix Section 4).

362 Since this reaction is central to the synthesis of all dNTPs, it is reasonable to consider the abundance  
 363 of these complexes is a measure of the total dNTP production in *E. coli*. Illustrated schematically in **Figure 6** (A), we consider the fact that to replicate the cell's genome, on the order of  $\approx 10^7$   
 364 dNTPs must be synthesized. Assuming a production rate of 10 per second per ribonucleotide  
 365 reductase complex and a cell division time of 6000 seconds, we arrive at an estimate of  $\approx 150$  com-  
 366 plexes needed per cell. As shown in the bottom panel of **Figure 6** (A), this estimate agrees with the  
 367 experimental measurements of these complexes abundances within  $\approx 1/2$  an order of magnitude.  
 368

369 Recent work has revealed that during replication, the ribonucleotide reductase complexes co-  
 370 alesce to form discrete foci colocalized with the DNA replisome complex (*Sánchez-Romero et al.*,  
 371 2011). This is particularly pronounced in conditions where growth is slow, indicating that spatial  
 372 organization and regulation of the activity of the complexes plays an important role.

### 373 DNA Replication

374 We now turn our focus to the integration of these dNTP building blocks into the replicated chromo-  
 375 some strand via the DNA polymerase. Replication is initiated at a single region of the chromosome  
 376 termed the *oriC* locus at which a pair of DNA polymerases bind and begin their high-fidelity repli-  
 377 cation of the genome in opposite directions. Assuming equivalence between the two replication  
 378 forks, this means that the two DNA polymerase complexes (termed replisomes) meet at the mid-  
 379 way point of the circular chromosome termed the *ter* locus. The kinetics of the five types of DNA  
 380 polymerases (I – V) have been intensely studied, revealing that DNA polymerase III performs the

381 high fidelity processive replication of the genome with the other "accessory" polymerases playing  
 382 auxiliary roles (*Fijalkowska et al., 2012*). *In vitro* measurements have shown that DNA Polymerase  
 383 III copies DNA at a rate of  $\approx$  600 nucleotides per second (BNID: 104120, *Milo et al. (2010)*). There-  
 384 fore, to replicate a single chromosome, two replisomes moving at their maximal rate would copy  
 385 the entire genome in  $\approx$  4000 s. Thus, with a division time of 5000 s (our "typical" growth rate for  
 386 the purposes of this work), there is sufficient time for a pair of DNA polymerase III complexes to  
 387 replicate the entire genome. However, this estimate implies that 4000 s would be the upper-limit  
 388 time scale for bacterial division which is at odds with the familiar 20 minute (1200 s) doubling time  
 389 of *E. coli* in rich medium.

390 It is well known that *E. coli* can parallelize its DNA replication such that multiple chromosomes  
 391 are being replicated at once, with as many as 10 - 12 replication forks at a given time (*Bremer*  
 392 and *Dennis, 2008*; *Si et al., 2017*). Thus, even in rapidly growing cultures, we expect only a few  
 393 polymerases ( $\approx$  10) are needed to replicate the chromosome per cell doubling. However, as shown  
 394 in *Figure 6(B)*, DNA polymerase III is nearly an order of magnitude more abundant. This  
 395 discrepancy can be understood by considering its binding constant to DNA. DNA polymerase III is  
 396 highly processive, facilitated by a strong affinity of the complex to the DNA. *In vitro* biochemical  
 397 characterization has quantified the  $K_D$  of DNA polymerase III holoenzyme to single-stranded and  
 398 double-stranded DNA to be 50 and 200 nM, respectively (*Ason et al., 2000*). The bottom plot in  
 399 *Figure 6* (B) shows that the concentration of the DNA polymerase III across all data sets and growth  
 400 conditions is within this range. Thus, while the copy number of the DNA polymerase III is in excess  
 401 of the strict number required to replicate the genome, its copy number appears to vary such that its  
 402 concentration is approximately equal to the dissociation constant to the DNA. While the processes  
 403 regulating the initiation of DNA replication are complex and involve more than just the holoenzyme,  
 404 these data indicate that the kinetics of replication rather than the explicit copy number of the DNA  
 405 polymerase III holoenzyme is the more relevant feature of DNA replication to consider. In light  
 406 of this, the data in *Figure 6(B)* suggests that for bacteria like *E. coli*, DNA replication does not represent a rate-limiting step in cell division. However, it is worth noting that for bacterium like *C. crescentus* whose chromosomal replication is initiated only once per cell cycle (*Jensen et al., 2001*), the time to double their chromosome likely represents an upper limit to their growth rate.

#### 410 RNA Synthesis

411 With the machinery governing the replication of the genome accounted for, we now turn our attention  
 412 to the next stage of the central dogma – the transcription of DNA to form RNA. We primarily  
 413 consider three major groupings of RNA, namely the RNA associated with ribosomes (rRNA), the  
 414 RNA encoding the amino-acid sequence of proteins (mRNA), and the RNA which links codon sequence  
 415 to amino-acid identity during translation (tRNA). Despite the varied function of these RNA species,  
 416 they share a commonality in that they are transcribed from DNA via the action of RNA polymerase. In the coming paragraphs, we will consider the synthesis of RNA as a rate limiting  
 417 step in bacterial division by estimating how many RNA polymerases must be present to synthesize  
 418 all necessary rRNA, mRNA, and tRNA.

#### 420 rRNA

421 We begin with an estimation of the number of RNA polymerases needed to synthesize the rRNA  
 422 that serve as catalytic and structural elements of the ribosome. Each ribosome contains three rRNA  
 423 molecules of lengths 120, 1542, and 2904 nucleotides (BNID: 108093, *Milo et al. (2010)*), meaning  
 424 each ribosome contains  $\approx$  4500 nucleotides. As the *E. coli* RNA polymerase transcribes DNA to  
 425 RNA at a rate of  $\approx$  40 nucleotides per second (BNID: 101904, *Milo et al. (2010)*), it takes a single RNA  
 426 polymerase  $\approx$  100 s to synthesize the RNA needed to form a single functional ribosome. Therefore,  
 427 in a 5000 s division time, a single RNA polymerase transcribing rRNA at a time would result in only  
 428  $\approx$  50 functional ribosomal rRNA units – far below the observed number of  $\approx$   $10^4$  ribosomes per cell.

429 Of course, there can be more than one RNA polymerase transcribing the rRNA genes at any

430 given time. To elucidate the *maximum* number of rRNA units that can be synthesized given a single  
 431 copy of each rRNA gene, we will consider a hypothesis in which the rRNA operon is completely tiled  
 432 with RNA polymerase. *In vivo* measurements of the kinetics of rRNA transcription have revealed  
 433 that RNA polymerases are loaded onto the promoter of an rRNA gene at a rate of  $\approx 1$  per second  
 434 (BNID: 111997; 102362, *Milo et al. (2010)*). If RNA polymerases are being constantly loaded on  
 435 to the rRNA genes at this rate, then we can assume that  $\approx 1$  functional rRNA unit is synthesized  
 436 per second. With a 5000 second division time, this hypothesis leads to a maximal value of 5000  
 437 functional rRNA units, still undershooting the observed number of  $10^4$  ribosomes per cell.

438 *E. coli* has evolved a clever mechanism to surpass this kinetic limit for the rate of rRNA produc-  
 439 tion. Rather than having only one copy of each rRNA gene, *E. coli* has seven copies of the operon  
 440 (BIND: 100352, *Milo et al. (2010)*) four of which are localized directly adjacent to the origin of repli-  
 441 cation (*Birnbaum and Kaplan, 1971*). As fast growth also implies an increased gene dosage due to  
 442 paralellized chromosomal replication, the total number of rRNA genes can be on the order of  $\approx 10$   
 443 – 70 copies at moderate to fast growth rates (*Stevenson and Schmidt, 2004*). Using our standard  
 444 time scale of a 5000 second division time, we can make the lower-bound estimate that the typical  
 445 cell will have 7 copies of the rRNA operon. Synthesizing one functional rRNA unit per second per  
 446 rRNA operon, a total of  $4 \times 10^4$  rRNA units can be synthesized, comfortably above the observed  
 447 number of ribosomes per cell.

448 How many RNA polymerases are then needed to constantly transcribe 7 copies of the rRNA  
 449 genes? We approach this estimate by considering the maximum number of RNA polymerases tiled  
 450 along the rRNA genes with a loading rate of 1 per second and a transcription rate of 40 nucleotides  
 451 per second. Considering that a RNA polymerase has a physical footprint of approximately 40 nu-  
 452 cleotides (BNID: 107873, *Milo et al. (2010)*), we can expect  $\approx 1$  RNA polymerase per 80 nucleotides.  
 453 With a total length of  $\approx 4500$  nucleotides per operon and 7 operons per cell, the maximum number  
 454 of RNA polymerases that can be transcribing rRNA at any given time is  $\approx 400$ . As we will see in the  
 455 coming sections, the synthesis of rRNA is the dominant requirement of the RNA polymerase pool.

#### 456 mRNA

457 To form a functional protein, all protein coding genes must first be transcribed from DNA to form  
 458 an mRNA molecule. While each protein requires an mRNA blueprint, many copies of the protein  
 459 can be synthesized from a single mRNA. Factors such as strength of the ribosomal binding site,  
 460 mRNA stability, and rare codon usage frequency dictate the number of proteins that can be made  
 461 from a single mRNA, with yields ranging from  $10^1$  to  $10^4$  (BNID: 104186; 100196; 106254, *Milo et al.*  
 462 (2010)). Computing the geometric mean of this range yields  $\approx 1000$  proteins synthesized per mRNA,  
 463 a value that agrees with experimental measurements of the number of proteins per cell ( $\approx 3 \times 10^6$ ,  
 464 BNID: 100088, *Milo et al. (2010)*) and total number of mRNA per cell ( $\approx 3 \times 10^3$ , BNID:100064, *Milo*  
 465 *et al. (2010)*).

466 This estimation captures the *steady-state* mRNA copy number, meaning that at any given time,  
 467 there will exist approximately 3000 unique mRNA molecules. To determine the *total* number of  
 468 mRNA that need to be synthesized over the cell's lifetime, we must consider degradation of the  
 469 mRNA. In most bacteria, mRNAs are rather unstable with life times on the order of several minutes  
 470 (BNID: 104324; 106253; 111927; 111998, *Milo et al. (2010)*). For convenience, we assume that the  
 471 typical mRNA in our cell of interest has a typical lifetime of  $\approx 300$  seconds. Using this value, we  
 472 can determine the total mRNA production rate to maintain a steady-state copy number of 3000  
 473 mRNA per cell. While we direct the reader to the appendix for a more detailed discussion of mRNA  
 474 transcriptional dynamics, we state here that the total mRNA production rate must be on the order  
 475 of  $\approx 15$  mRNA per second. In *E. coli*, the average protein is  $\approx 300$  amino acids in length (BNID:  
 476 108986; *Milo et al. (2010)*), meaning that the corresponding mRNA is  $\approx 900$  nucleotides which we  
 477 will further approximate as  $\approx 1000$  nucleotides to account for the non-protein coding regions on  
 478 the 5' and 3' ends. This means that the cell must have enough RNA polymerase molecules about  
 479 to sustain a transcription rate of  $\approx 1.5 \times 10^4$  nucleotides per second. Knowing that a single RNA

<sup>480</sup> polymerase polymerizes RNA at a clip of 40 nucleotides per second, we arrive at a comfortable  
<sup>481</sup> estimate of  $\approx 250$  RNA polymerase complexes needed to satisfy the mRNA demands of the cell. It  
<sup>482</sup> is worth noting that this number is approximately half of that required to synthesize enough rRNA,  
<sup>483</sup> as we saw in the previous section. We find this to be a striking result as these 250 RNA polymerase  
<sup>484</sup> molecules are responsible for the transcription of the  $\approx 4000$  protein coding genes that are not  
<sup>485</sup> ribosome associated.

#### <sup>486</sup> tRNA

<sup>487</sup> The final class of RNA molecules worthy of quantitative consideration is the the pool of tRNAs  
<sup>488</sup> used during translation to map codon sequence to amino acid identity. Unlike mRNA or rRNA,  
<sup>489</sup> each individual tRNA is remarkably short, ranging from 70 to 95 nucleotides each (BNID: 109645;  
<sup>490</sup> 102340, *Milo et al. (2010)*). What they lack in length, they make up for in abundance. There are  
<sup>491</sup> approximately  $\approx 3000$  tRNA molecules present for each of the 20 amino acids (BNID: 105280, *Milo*  
<sup>492</sup> *et al. (2010)*), although the precise copy number is dependent on the identity of the ligated amino  
<sup>493</sup> acid. Using these values, we make the estimate that  $\approx 5 \times 10^6$  nucleotides are sequestered in tRNA  
<sup>494</sup> per cell. Unlike mRNA, tRNA is remarkably stable with typical lifetimes *in vivo* on the order of  $\approx 48$   
<sup>495</sup> hours (*Abelson et al., 1974; Svennningsen et al., 2017*) – well beyond the timescale of division. Once  
<sup>496</sup> again using our rule-of-thumb for the rate of transcription to be 40 nucleotides per second and  
<sup>497</sup> assuming a division time of  $\approx 5000$  seconds, we arrive at an estimate of  $\approx 20$  RNA polymerases  
<sup>498</sup> to synthesize enough tRNA. This requirement pales in comparison to the number of polymerases  
<sup>499</sup> needed to generate the rRNA and mRNA pools and can be neglected as a significant transcriptional  
<sup>500</sup> burden.

#### <sup>501</sup> RNA Polymerase and $\sigma$ -factor Abundance

<sup>502</sup> These estimates, summarized in *Figure 7 (A)*, reveal that synthesis of rRNA and mRNA are the dominant  
<sup>503</sup> RNA species synthesized by RNA polymerase, suggesting the need for  $\approx 700$  RNA polymerases  
<sup>504</sup> per cell. As is revealed in *Figure 7 (B)*, this estimate is about an order of magnitude below the observed  
<sup>505</sup> number of RNA polymerase complexes per cell ( $\approx 5000 - 7000$ ). The disagreement between  
<sup>506</sup> the estimated number of RNA polymerases and these observations are at least consistent with  
<sup>507</sup> recent literature revealing that  $\approx 80\%$  of RNA polymerases in *E. coli* are not transcriptionally active  
<sup>508</sup> (*Patrick et al., 2015*). Our estimate ignores the possibility that some fraction is only nonspecifically  
<sup>509</sup> bound to DNA, as well as the obstacles that RNA polymerase and DNA polymerase present for each  
<sup>510</sup> other as they move along the DNA (*Finkelstein and Greene, 2013*).

<sup>511</sup> In addition, it is also vital to consider the role of  $\sigma$ -factors which help RNA polymerase identify  
<sup>512</sup> and bind to transcriptional start sites (*Browning and Busby, 2016*). Here we consider  $\sigma^{70}$  (RpoD)  
<sup>513</sup> which is the dominant "general-purpose"  $\sigma$ -factor in *E. coli*. While initially thought of as being solely  
<sup>514</sup> involved in transcriptional initiation, the past two decades of single-molecule work has revealed  
<sup>515</sup> a more multipurpose role for  $\sigma^{70}$  including facilitating transcriptional elongation (*Kapanidis et al., 2005; Goldman et al., 2015; Perdue and Roberts, 2011; Mooney and Landick, 2003; Mooney et al., 2005*). *Figure 7 (B)* is suggestive of such a role as the number of  $\sigma^{70}$  proteins per cell is in close  
<sup>517</sup> agreement with our estimate of the number of transcriptional complexes needed.

<sup>519</sup> While these estimates and comparison with experimental data reveal an interesting dynamic  
<sup>520</sup> at play between the transcriptional demand and copy numbers of the corresponding machinery,  
<sup>521</sup> these findings illustrate that transcription cannot be the rate limiting step in bacterial division. *Figure 7 (A)* reveals that the availability of RNA polymerase is not a limiting factor for cell division as the  
<sup>523</sup> cell always has an apparent  $\sim 10$ -fold excess than needed. Furthermore, if more transcriptional  
<sup>524</sup> activity was needed to satisfy the cellular requirements, more  $\sigma^{70}$ -factors could be expressed to  
<sup>525</sup> utilize a larger fraction of the RNA polymerase pool.

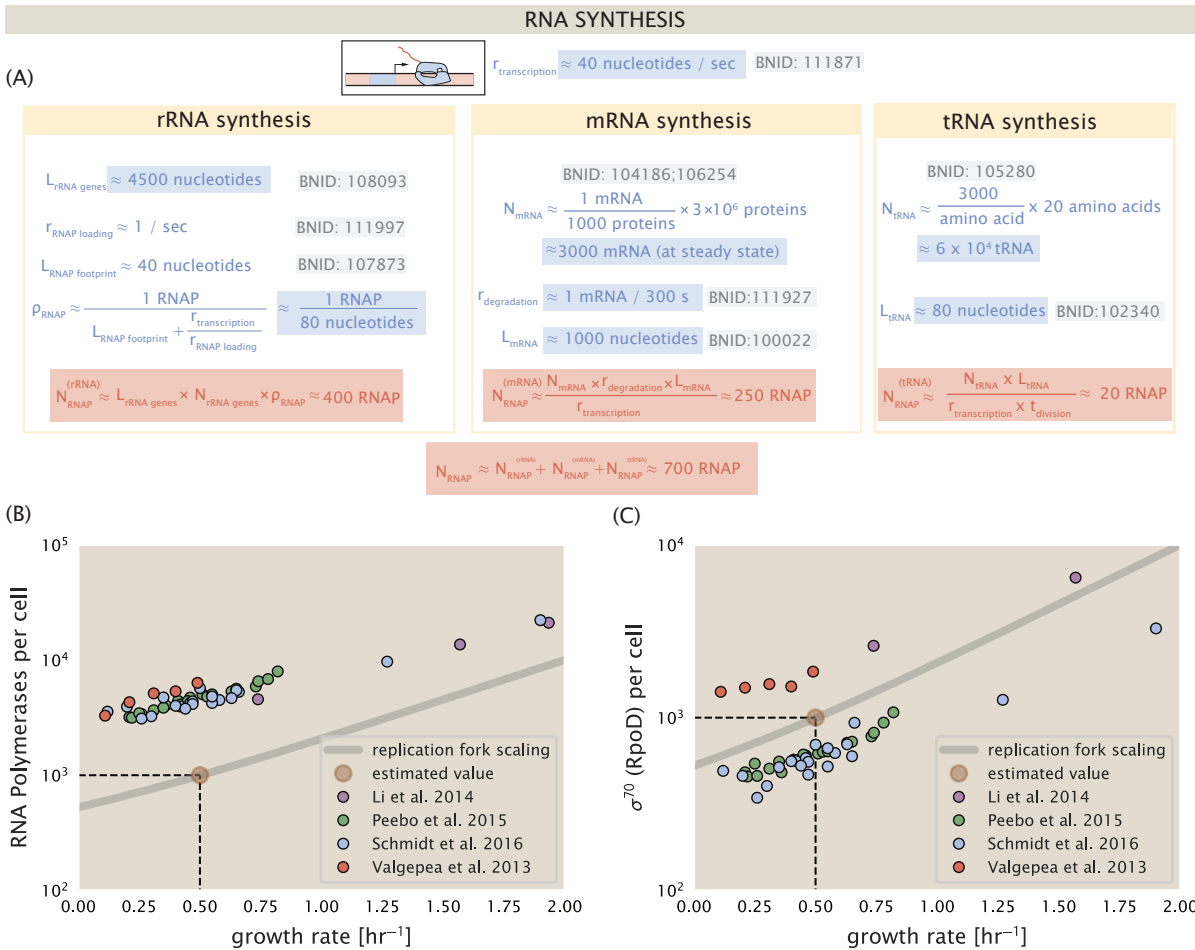


**Figure 7. Estimation of the RNA polymerase demand and comparison with experimental data.** (A) Estimations for the number of RNA polymerase needed to synthesize sufficient quantities of rRNA, mRNA, and tRNA from left to right, respectively. Bionumber Identifiers (BNIDs) are provided for key quantities used in the estimates. (B) The RNA polymerase core enzyme copy number as a function of growth rate. Colored points correspond to the average number RNA polymerase core enzymes that could be formed given a subunit stoichiometry of  $[RpoA]_2[RpoC][RpoB]$ . (C) The abundance of  $\sigma^{70}$  as a function of growth rate. Estimated value for the number of RNAP is shown in (B) and (C) as a translucent brown point at a growth rate of  $0.5 \text{ hr}^{-1}$ .

**526 Translation and ribosomal synthesis**

527 Lastly, we turn our attention to the process of synthesizing new proteins, translation. These pro-  
 528 cesses stand as good candidates for defining the growth limit as the synthesis of new proteins  
 529 relies on the generation of ribosomes, themselves proteinaceous molecules. As we will see in the  
 530 coming sections of this work, this poses a "chicken-or-the-egg" problem where the synthesis of  
 531 ribosomes requires ribosomes in the first place.

532 We will begin our exploration of protein translation in the same spirit as we have in previous  
 533 sections – we will draw order-of-magnitude estimates based on our intuition and relying on litera-  
 534 ture studies and will compare these estimates to the observed data. In doing so, we will estimate  
 535 both the absolute number of ribosomes necessary for replication of the proteome as well as the  
 536 synthesis of amino-acyl tRNAs. In the closing sections, we will explore the details of ribosome bio-  
 537 genesis in granular detail, ultimately presenting a quantitative model tying ribosome abundance  
 538 to the concentration of amino acids as well as the state of chromosome replication.

**539 tRNA synthetases**

540 We begin by first estimating the number of tRNA ligases in *E. coli* needed to convert free amino-  
 541 acids to polypeptide chains. At a modest growth rate of  $\approx 5000$  s, *E. coli* has roughly  $3 \times 10^6$  proteins  
 542 per cell (BNID: 115702; *Milo et al. (2010)*). Assuming that the typical protein is on the order of  $\approx$   
 543 300 amino acids in length (BNID: 100017; *Milo et al. (2010)*), we can estimate that a total of  $\approx 10^9$   
 544 amino acids are stitched together by peptide bonds.

545 How many tRNAs are needed to facilitate this remarkable number of amino acid delivery events  
 546 to the translating ribosomes? It is important to note that tRNAs are recycled after they've passed  
 547 through the ribosome and can be recharged with a new amino acid, ready for another round of  
 548 peptide bond formation. While some *in vitro* data exists on the turnover of tRNA in *E. coli* for  
 549 different amino acids, we can make a reasonable estimate by comparing the number of amino  
 550 acids to be polymerized to cell division time. Using our stopwatch of 5000 s and  $10^9$  amino acids,  
 551 we arrive at a requirement of  $\approx 2 \times 10^5$  tRNA molecules. This estimate is in line with experimental  
 552 measurements of  $\approx 3 \times 10^5$  per cell (BNID: 108611, *Milo et al. (2010)*), suggesting we are on the  
 553 right track.

554 There are many processes which go into synthesizing a tRNA and ligating it with the appropriate  
 555 amino acids. As we covered in the previous section, there appear to be more than enough RNA  
 556 polymerases per cell to synthesize the needed pool of tRNAs. Without considering the many ways  
 557 in which amino acids can be scavenged or synthesized *de novo*, we can explore ligation the as a  
 558 potential rate limiting step. The enzymes which link the correct amino acid to the tRNA, known as  
 559 tRNA synthetases or tRNA ligases, are incredible in their proofreading of substrates with the incor-  
 560 rect amino acid being ligated once out of every  $10^4$  to  $10^5$  times (BNID: 103469, *Milo et al. (2010)*).  
 561 This is due in part to the consumption of energy as well as a multi-step pathway to ligation. While  
 562 the rate at which tRNA is ligated is highly dependent on the identity of the amino acid, it is reason-  
 563 able to state that the typical tRNA synthetase has charging rate of  $\approx 20$  AA per tRNA synthetase per  
 564 second (BNID: 105279, *Milo et al. (2010)*).

565 Combining these estimates together, as shown schematically in **Figure 8(A)**, yields an estimate  
 566 of  $\approx 10^4$  tRNA synthetases per cell with a division time of 5000 s. This point estimate is in very close  
 567 agreement with the observed number of synthetases (the sum of all 20 tRNA synthetases in *E. coli*).  
 568 This estimation strategy seems to adequately describe the observed growth rate dependence of  
 569 the tRNA synthetase copy number (shown as the grey line in **Figure 8(B)**), suggesting that the copy  
 570 number scales with the cell volume.

571 In total, the estimated and observed  $\approx 10^4$  tRNA synthetases occupy only a meager fraction of  
 572 the total cell proteome, around 0.5% by abundance. It is reasonable to assume that if tRNA charg-  
 573 ing was a rate limiting process, cells would be able to increase their growth rate by devoting more  
 574 cellular resources to making more tRNA synthases. As the synthesis of tRNAs and the correspond-  
 575 ing charging can be highly parallelized, we can argue that tRNA charging is not a rate limiting step

576 in cell division, at least for the growth conditions explored in this work.

577 **Protein synthesis**

578 With the number of tRNA synthetases accounted for, we now consider the abundance of the pro-  
 579 tein synthesis machines themselves, ribosomes. Ribosomes are enormous protein/rRNA com-  
 580 plexes that facilitate the peptide bond formation between amino acids in the correct sequence  
 581 as defined by the coding mRNA. Before we examine the synthesis of the ribosome proteins and  
 582 the limits that may place on the observed bacterial growth rates, let's consider replication of the  
 583 cellular proteome.

584 As described in the previous section, *E. coli* consists of  $\approx 3 \times 10^6$  proteins at a growth rate of  $\approx$   
 585 5000 s. If we again assume that each protein is composed of  $\approx 300$  amino acids and each amino  
 586 acid is linked together by one peptide bond, we arrive at an estimate that the cellular proteome  
 587 consists of  $\approx 10^{10}$  peptide bonds. While the rate at which ribosomes translates is well known to  
 588 have a growth rate dependence *Dai et al. (2018)* and is a topic which we discuss in detail in the  
 589 coming sections. However, for the purposes of our order-of-magnitude estimate, we can make  
 590 the approximation that translation occurs at a rate of  $\approx 15$  amino acids per second per ribosome  
 591 (BNID: 100233, *Milo et al. (2010)*). Under this approximation and assuming a division time of 5000  
 592 s, we can arrive at an estimate of  $\approx 10^4$  ribosomes are needed to replicate the cellular proteome,  
 593 shown in *Figure 8(B)*. This point estimate, while glossing over important details such as chromo-  
 594 some copy number and growth-rate dependent translation rates, proves to be notably accurate  
 595 when compared to the experimental observations (*Figure 8(B)*).

596 **Translation as a growth-rate limiting step**

597 Thus far in our work, the general back-of-the-envelope estimates have been reasonably successful  
 598 in explaining what sets the scale of absolute protein copy number. In many cases, these estimates  
 599 can be adapted to consider a continuum of growth rates in lieu of a single 5000 s point estimate,  
 600 the details of which are described in the Supplemental Information. A recurring theme we have  
 601 relied on is the ability of the cell to parallelize different processes to transport or synthesize the  
 602 required amount of the corresponding biomolecule. For example, we saw in our example of *E. coli*  
 603 grown on different carbon sources that expression of particular transporters can be induced, often  
 604 producing more than needed acquire enough carbon to build new cell mass (??(B)). In examining  
 605 replication of the DNA, we described how cells can replicate multiple copies of the chromosome  
 606 at any given time, permitting growth rates faster than the limit at which the chromosome can be  
 607 faithfully replicated. As a final example, we showed how increasing the gene dosage of the rRNA  
 608 operons is necessary to produce enough rRNA to form functional ribosomes. However, when it  
 609 comes to ribosome biogenesis, namely the translation of ribosomal proteins, such parallelization  
 610 is not possible, suggesting that translation may be a key factor determining the cellular growth  
 611 rate.

612 Optimal resource allocation and the role of ribosomal proteins have been an area of intense  
 613 quantitative study over the last decade by Hwa and others (*Scott et al., 2010; Hui et al., 2015*).  
 614 From the perspective of limiting growth, our earlier estimate of rRNA highlighted the necessity for  
 615 multiple copies of rRNA genes in order to make enough rRNA. For *E. coli*'s fastest growth rates at  
 616  $2 \text{ hr}^{-1}$ , the additional demand for rRNA is further supported by parallelized DNA replication and  
 617 increased rRNA gene dosage. This suggests the possibility that synthesis of ribosomes might be  
 618 rate limiting. While the transcriptional demand for the ribosomal proteins is substantially lower  
 619 than rRNA genes, since proteins can be translated from relatively fewer mRNA, other ribosomal  
 620 proteins like the translation elongation factor EF-Tu also present a substantial burden. For EF-Tu  
 621 in particular, it is the most highly expressed protein in *E. coli* and is expressed from multiple gene  
 622 copies, *tufA* and *tufB*.

623 To gain some intuition into how translation may set the speed limit for bacterial growth, we  
 624 again consider the total number of peptide bonds that must be synthesized,  $N_{\text{AA}}$ . Noting that cell

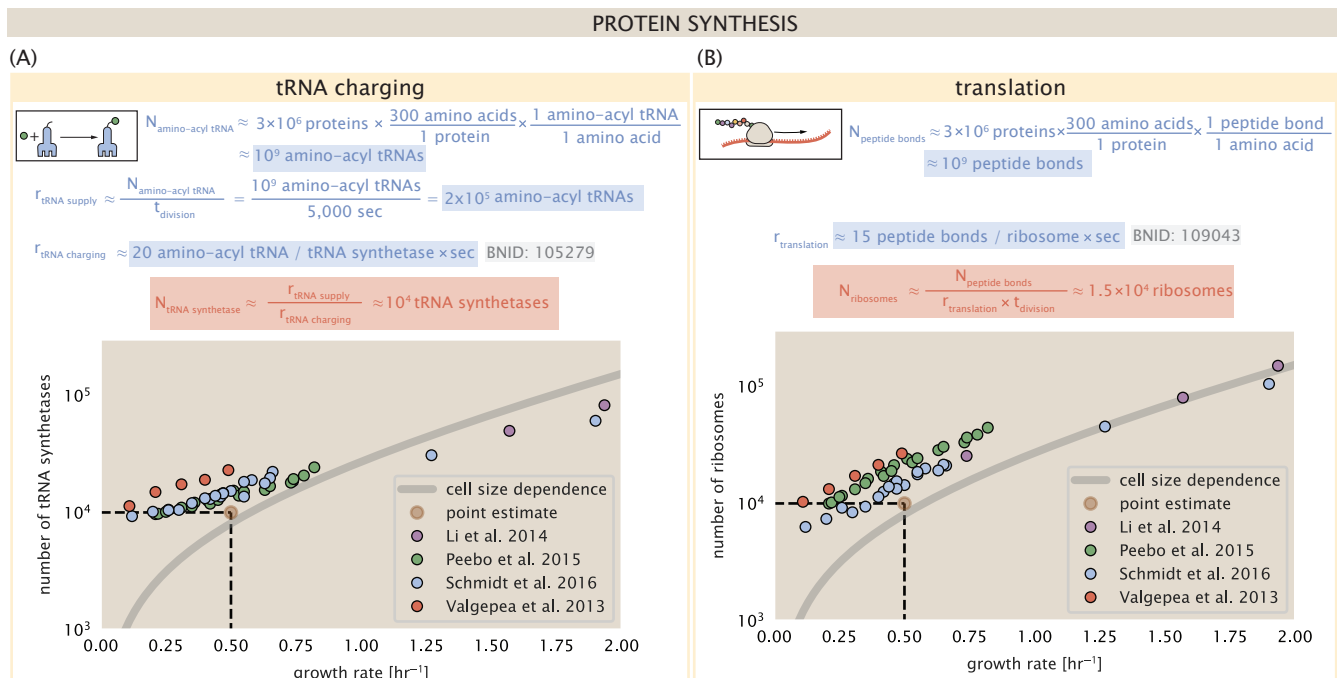


**Figure 8. Estimation of the required tRNA synthetases and ribosomes.** (A) Estimation for the number of tRNA synthetases that will supply the required amino acid demand. The sum of all tRNA synthetases copy numbers are plotted as a function of growth rate ([ArgS], [CysS], [GlnS], [Glx], [IleS], [LeuS], [ValS], [AlaS]<sub>2</sub>, [AsnS]<sub>2</sub>, [AspS]<sub>2</sub>, [TyrS]<sub>2</sub>, [TrpS]<sub>2</sub>, [ThrS]<sub>2</sub>, [SerS]<sub>2</sub>, [ProS]<sub>2</sub>, [PheS]<sub>2</sub>[PheT]<sub>2</sub>, [MetG]<sub>2</sub>, [LysS]<sub>2</sub>, [HisS]<sub>2</sub>, [GlyS]<sub>2</sub>[GlyQ]<sub>2</sub>). (B) Estimation of the number of ribosomes required to synthesize 10<sup>9</sup> peptide bonds with an elongation rate of 15 peptide bonds per second. The average abundance of ribosomes is plotted as a function of growth rate. Our estimated values are shown for a growth rate of 0.5 hr<sup>-1</sup>. Grey lines correspond to the estimated complex abundance calculated at different growth rates. See Supplemental Information XX for a more detail description of this calculation.

625 mass grows exponentially (**Godin et al., 2010**), we can compute the number of amino acids to be  
 626 polymerized as

$$N_{AA} = \frac{r_t R}{\lambda}, \quad (1)$$

627 where  $\lambda$  is the cell growth rate in  $s^{-1}$ ,  $r_t$  is the maximum translation rate in amino acids per second,  
 628 and  $R$  is the average ribosome copy number per cell. Knowing the number of peptide bonds to be  
 629 formed permits us to compute the translation-limited growth rate as

$$\lambda_{\text{translation-limited}} = \frac{r_t R}{N_{AA}}. \quad (2)$$

630 Alternatively, since  $N_{AA}$  is related to the total protein mass through the molecular weight of  
 631 each protein, we can also consider the growth rate in terms of the fraction of the total proteome  
 632 mass that is dedicated to ribosomal protein mass. By making the approximation that an average  
 633 amino acid has a molecular weight of 110 Da (see **Figure 9(A)**), we can rewrite the growth rate as,

$$\lambda_{\text{translation-limited}} \approx \frac{r_t}{L_R} \Phi_R, \quad (3)$$

634 where  $L_R$  is the total length in amino acids that make up a ribosome, and  $\Phi_R$  is the ribosomal mass  
 635 fraction. This is plotted as a function of ribosomal fraction  $\Phi_R$  in **Figure 9(A)**, where we take  $L_R \approx$   
 636 7500 aa, corresponding to the length in amino acids for all ribosomal subunits of the 50S and 30S  
 637 complex (BNID: 101175, (**Milo et al., 2010**)). This formulation assumes that the cell can transcribe  
 638 the required amount of rRNA, which appears reasonable for *E. coli*, allowing us to consider the  
 639 inherent limit on growth set by the ribosome.

640 The growth rate defined by Equation 3 reflects mass-balance under steady-state growth and  
 641 has long provided a rationalization to the apparent linear increase in *E. coli*'s ribosomal content  
 642 as a function of growth rate (**Maaløe, 1979; Scott et al., 2010**). For our purposes, there are several  
 643 important consequences of this trend. Firstly, we note there is a maximum growth rate of  $\lambda \approx$   
 644  $6hr^{-1}$ , or doubling time of about 7 minutes (dashed line). This growth rate can be viewed as an  
 645 inherent maximum growth rate due to the need for the cell to double the cell's entire ribosomal  
 646 mass. Interestingly, this limit is independent of the absolute number of ribosomes and is simply  
 647 given by time to translate an entire ribosome,  $L_R/r_t$ . As shown in **Figure 9(B)**, we can reconcile this  
 648 with the observation that in order to double the average number of ribosomes, each ribosome  
 649 must produce a second ribosome. Unlike DNA replication or rRNA transcription, this is a process  
 650 that cannot be parallelized.

651 For reasonable values of  $\Phi_R$ , between about 0.1 - 0.3 (**Scott et al., 2010**), the maximum growth  
 652 rate is in line with experimentally reported growth rates around 0.5 - 2  $hr^{-1}$ . Importantly, in order  
 653 for a cell to increase their growth limit they *must* increase their relative ribosomal abundance. This  
 654 can be achieved by either synthesizing more ribosomes or reducing the fraction of non-ribosomal  
 655 proteins. Reduction of non-ribosomal proteins is not a straightforward task since (as we have  
 656 found throughout our estimates) doubling a cell requires many other enzymes and transporters.  
 657 Increasing the absolute ribosomal abundance in *E. coli* will be limited by the number of rRNA oper-  
 658 ons.

659 Here we again return to rRNA synthesis, but here consider the maximum rRNA that can be  
 660 produced at different growth rates.

661 [expand on.]

## 662 Discussion

663 [Fill in.]

### 664 Maximizing growth rate requires coordination of biosynthesis at all growth rates.

665 However, the mechanism behind growth rate control has remained elusive and has only been  
 666 described at a phenomenological level.

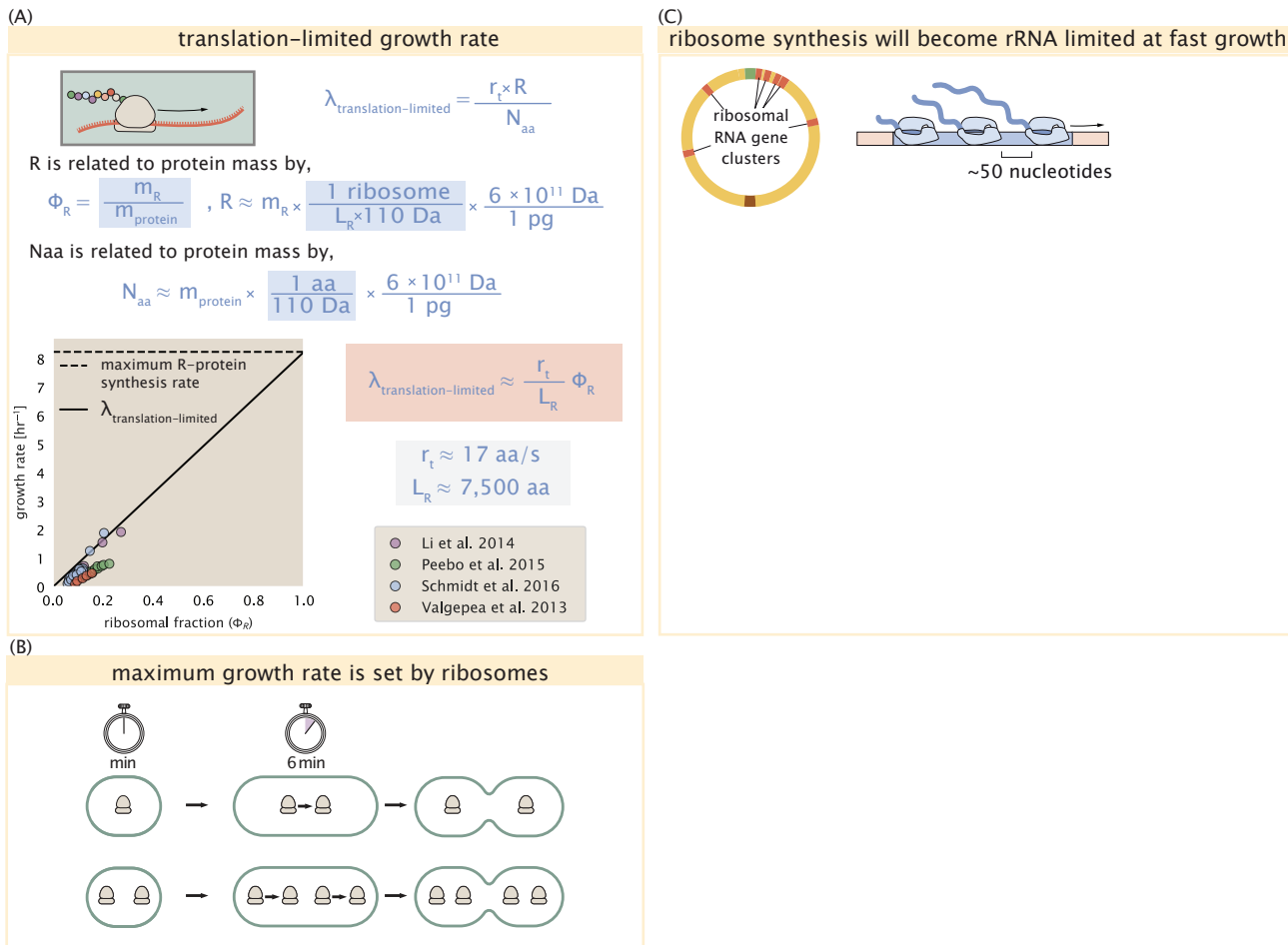


**Figure 9. Translation-limited growth rate.** (A) Here we consider the translation-limited growth as a function of ribosomal fraction. By mass balance, the time required to double the entire proteome ( $N_{AA} / r_t$ ) sets the translation-limited growth rate,  $\lambda_{\text{translation-limited}}$ . Here  $N_{aa}$  is effectively the number of peptide bonds that must be translated,  $r_t$  is the translation elongation rate, and  $R$  is the number of ribosomes. This can also be re-written in terms of the ribosomal mass fraction  $\Phi_R = m_R / m_{\text{protein}}$ , where  $m_R$  is the total ribosomal mass and  $m_{\text{protein}}$  is the mass of all proteins in the cell.  $L_R$  refers to the summed length of the ribosome in amino acids.  $\lambda_{\text{translation-limited}}$  is plotted as a function of  $\Phi_R$  (solid line). (B) The dashed line in part (A) identifies a maximum growth rate that is set by the ribosome. Specifically, this growth rate corresponds to the time required to translate an entire ribosome,  $L_R / r_t$ . This is a result that is independent of the number of ribosomes in the cell as shown schematically here. (C)

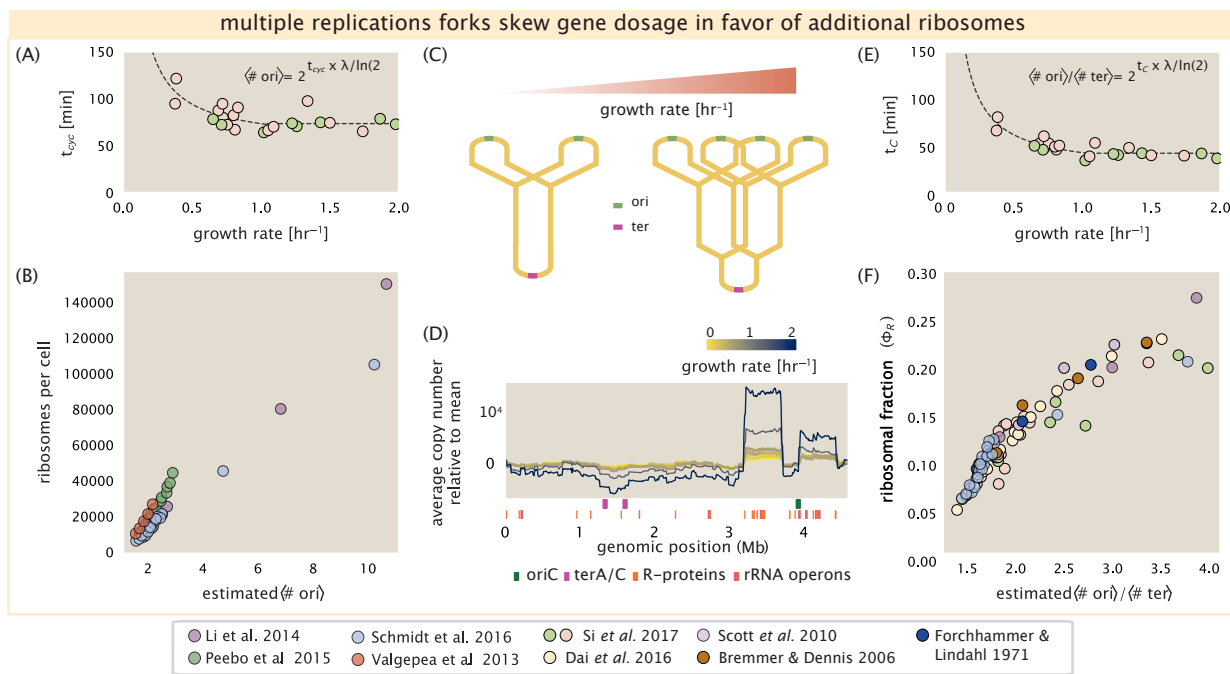


**Figure 10. Multiple replication forks skew gene dosage and ribosomal content.** (A) Schematic shows the expected increase in replication forks (or number of ori regions) as *E. coli* cells grow faster. (B) A running boxcar average of protein copy number is calculated for each each growth condition considered by Schmidt *et al.*. A 0.5 Mb averaging window was used. Protein copy numbers are reported relative to their condition-specific means in order to center all data sets. (C) and (E) show experimental data from Si *et al.* (2017) Solid lines show fits to the data, which were used to estimate  $\langle \# \text{ori} \rangle / \langle \# \text{ter} \rangle$  and  $\langle \# \text{ori} \rangle$  [NB: to note fit equations]. Red data points correspond to measurements in strain MG1655, while light green points are for strain NCM3722. (D) Plot compares our estimate of  $\langle \# \text{ori} \rangle / \langle \# \text{ter} \rangle$  to the experimental measurements of ribosomal abundance. Ribosomal fraction was approximated from the RNA/protein ratios of Dai *et al.* (2016) (yellow) and Si *et al.* (2017) (light red and light green) by the conversion RNA/protein ratio  $\approx \Phi_R \cdot 2.1$ . (F) Plot of the ribosome copy number estimated from the proteomic data against the estimated  $\langle \# \text{ori} \rangle$ .

667 Here we attempt to place our observations across the proteomic data sets in the context of *E.*  
 668 *coli* maximizing its steady-state growth rate across a wide array of conditions.

669 Parallel DNA replication biases gene dosage in support of ribosome synthesis.  
 670 *E. coli* cells grow by a so-called "adder" mechanism, whereby cells add a constant volume with  
 671 each cell division (Taheri-Araghi *et al.*, 2015). In conjunction with this, additional rounds of DNA  
 672 replication are triggered when cells reach a critical volume per origin of replication (Figure 10(A)).  
 673 This leads to the classically-described exponential increase in cell size with growth rate Schaechter  
 674 *et al.* (1958); Si *et al.* (2017, 2019). In the context of maximizing growth rate, it is notable that the  
 675 majority of ribosomal proteins and rRNA operons are found closer to the DNA origin.

676 While an increase in transcription has been observed for genes closer to the origin in rapidly  
 677 growing *E. coli* (Scholz *et al.*, 2019), we were unaware of such characterization at the proteomic  
 678 level. In order to see whether there is a relative increase in protein expression for genes closer to  
 679 the origin at faster growth, we calculated a running boxcar average (500 kbp window) of protein  
 680 copy number as a function of each gene's transcriptional start site (Figure 10(B)). While absolute  
 681 protein copy numbers can vary substantially across the chromosome, we indeed observe a bias in  
 682 expression under fast growth conditions (dark blue), showing the result. The dramatic change in  
 683 protein copy number near the origin is primarily due to the increase in ribosomal protein expres-  
 684 sion. This trend is in contrast to slower growth conditions (yellow) where the average copy number  
 685 is more uniform across the length of the chromosome.

686 If ribosomal genes (rRNA and ribosomal proteins) are being synthesized at their maximal rate  
 687 according to their rRNA gene dosage and maximal transcription rate, we can make two related  
 688 hypotheses about how their ribosome abundance should vary with chromosomal content. First,  
 689 the ribosomal protein fraction should increase in proportion to the average ratio of DNA origins to  
 690 DNA termini ( $\langle \# \text{ ori} \rangle / \langle \# \text{ ter} \rangle$  ratio). This is a consequence of the skew in DNA dosage as cells grow  
 691 faster. The second hypothesis is that the absolute number of ribosomes should increase with the  
 692 number of DNA origins ( $\langle \# \text{ ori} \rangle$ ), since this will reflect the total gene dosage at a particular growth  
 693 condition.

694 In order to test each of these expectations we considered the experimental data from *Si et al.*  
 695 (2017), which inferred these parameters for cells under nutrient-limited growth. The ratio  $\langle \# \text{ ori} \rangle /$   
 696  $\langle \# \text{ ter} \rangle$  depends on how quickly chromosomes are replicated relative the cell's doubling time  $\tau$  and  
 697 is given by  $2^{\tau_c/\tau}$ . Here  $\tau_c$  is the time taken to replicate *E. coli*'s chromosome, referred to as the C  
 698 period of cell division. In **Figure 10(C)** we plot the measured  $\tau_c$  versus  $\tau$  (computed as  $\tau = \log(2)/\lambda$ ),  
 699 with data points in red corresponding to *E. coli* strain MG1655, and blue to strain NCM3722. *Si*  
 700 *et al.* (2017) also measured the total RNA to protein ratio which reflects ribosomal abundance and  
 701 we show that data along with other recent measurements from *Dai et al.* (2016, 2018). Indeed, we  
 702 find that the ribosomal fraction increases with  $\langle \# \text{ ori} \rangle / \langle \# \text{ ter} \rangle$  (**Figure 10(C)**). We note a systematic  
 703 difference in the relative abundances from *Peebo et al.* (2015) and *Valgepea et al.* (2013) that was  
 704 inconsistent with a number of other measurements of total RNA-to-protein ratios ( $\approx \Phi_R \times 2.1$  *Dai*  
 705 *et al.* (2016)) and only show the data from *Schmidt et al.* (2016) and *Li et al.* (2014) for relative  
 706 ribosome abundances (see supplemental section XX for a more complete discussion). For the data  
 707 shown, the ribosomal fraction doesn't increase as much at higher  $\langle \# \text{ ori} \rangle / \langle \# \text{ ter} \rangle$ . Since several  
 708 rRNA operons are actually located approximately half-way between the origin and terminus, the  
 709 trend may in part be a consequence of a diminishing increase in rRNA gene dosage at higher  $\langle \#$   
 710  $\text{ori} \rangle / \langle \# \text{ ter} \rangle$  ratios.

711 We can similarly estimate  $\langle \# \text{ ori} \rangle$ , which depends on how often replication forks are initiated  
 712 per cell cycle. This is given by the number of overlapping cell cycles,  $2^{\tau_{\text{cyc}}/\tau}$ , where  $\tau_{\text{cyc}}$  refers to  
 713 the total time of chromosome replication and cell division. **Figure 10(E)** shows the associated data  
 714 from *Si et al.* (2019), which we use to estimate  $\langle \# \text{ ori} \rangle$  for each growth condition of the proteomic  
 715 data. In agreement with our expectations, we find that ribosome copy number increases with the  
 716 estimated  $\langle \# \text{ ori} \rangle$  (**Figure 10(F)**).

717 While it is difficult to distinguish between causality and correlation, the data is consistent with  
 718 the need for cells to increase their effective rRNA gene dosage in order to grow according to the  
 719 constraint set by Equation 2. These results may also shed some light on the notable increase  
 720 in ribosomal content that is observed when sublethal doses of antibiotics (*Scott et al.*, 2010; *Dai*  
 721 *et al.*, 2016). Specifically, if rRNA synthesis is rate limiting, and nutrient conditions largely dictate the  
 722 extent of overlapping DNA replication cycles, than addition of antibiotic will lengthen the doubling  
 723 time and allow an increased rRNA synthesis relative to the rate of cell division. In Supplemental  
 724 Section XX, we consider this further using additional data from *Si et al.* (2017).

725 Regulation of translating ribosomes helps maintain maximal growth according to nutrient  
 726 availability.

727 While the above observations show how *E. coli* can vary its ribosomal content to increase growth  
 728 rate, it also presents a challenge in the limit of poorer nutrient conditions. Recall from Equation 3  
 729 that ribosomal content should decrease to zero as growth decreases to zero. While bacteria tend to  
 730 decrease their ribosomal abundance in poorer nutrient conditions, they do so only to some fixed,  
 731 non-zero amount (*Scott et al.*, 2010; *Liebermeister et al.*, 2014). Here we find a minimal ribosomal  
 732 fraction of  $\approx 0.06$  in the slowest growth conditions. From the perspective of a bacterium dealing  
 733 with uncertain nutrient conditions, there is likely a benefit for the cell to maintain some relative  
 734 fraction of ribosomes to support rapid growth as nutrient conditions improve.

735 The challenge however, lies in the cell's ability to maintain growth when ribosomes are in ex-

cess of the rate that nutrients can be harvested and amino acids synthesized for consumption  
 736 **Figure 11A.** In the limit of poor growth conditions, ribosomes would consume their amino acid  
 737 supply and be unable to maintain steady-state growth. In reality, *E. coli* is still able to maintain a  
 738 relatively high elongation rate even in stationary phase ( $\approx 8$  AA/s, (Dai et al., 2016, 2018)). A explanation  
 739 for this is that the cell further regulates its biological activity in conditions of stress and  
 740 nutrient-limitation; in particular through the small-molecule alarmones (p)ppGpp (Harris and The-  
 741 riot, 2018). In (p)ppGpp null strains, cells are unable to grow in nutrient-poor media. Indeed, these  
 742 small molecules play a role in controlling biosynthesis rates throughout the central dogma [NB  
 743 citations]. Here we explore this further in the context of growth by maximizing protein synthesis.  
 744

We consider slow growth conditions ( $\lambda$  less than  $0.5 \text{ hr}^{-1}$ ) by assuming that the decrease in  
 745 elongation rate is due to a limiting supply of amino acids and a need for the cell to maintain ex-  
 746 cess nutrients for cellular homeostasis under steady-state growth. There is some experimental  
 747 support showing that in poorer nutrient growth conditions, cells have lower amino acids concen-  
 748 trations (Bennett et al., 2009). We proceed by coarse graining the cell's amino acid supply as an  
 749 single, effective rate-limiting species (see Supplemental Section XX for a more complete discussion).  
 750 Under such a scenario, the elongation rate can described as simply depending on the maximum  
 751 elongation rate ( $\approx 17.1$  aa/s, (Dai et al., 2016, 2018)), an effective  $K_d$ , and the limiting amino acid  
 752 concentration  $[AA]_{eff}$ . Specifically, the elongation rate is given by,

$$r_t = r_t^{max} \cdot \frac{1}{1 + K_d/[AA]_{eff}}. \quad (4)$$

753 For cells growing in minimal media + glucose, the amino acid concentration is of order 100 mM  
 754 (BNID: 110093, (Milo et al., 2010; Bennett et al., 2009)). With a growth rate of about  $0.6 \text{ hr}^{-1}$  and  
 755 elongation rate of 12.5 aa per second (Dai et al., 2016), we can estimate an effective  $K_d$  of about 40  
 756 mM. Ultimately the steady state amino acid concentration will depend on the difference between  
 757 the supply of amino acids  $r_{aa}$  and consumption by ribosomes  $r_t \cdot R \cdot f_a$ , where  $f_a$  accounts for the  
 758 possible reduction of actively translating ribosomes.

759 In **Figure 11B** we consider how the maximal growth rate and elongation rates vary as a func-  
 760 tion of the number of actively translating ribosomes in this slow growth regime (see Supplemen-  
 761 tal Section XX for a complete description of this model). If we consider  $r_{AA}$  to be reflective of a  
 762 specific growth condition, by considering lines of constant  $r_{AA}$ , we find that cells grow fastest by  
 763 maximizing their fraction of actively translating ribosomes. When we consider the experimental  
 764 measurements from Dai et al. (2018), we see that although cells indeed reduce  $R \times f_a$ , they do so  
 765 in a way that keeps  $[AA]_{eff}$  relatively constant. Given our estimate for the  $K_d$  of 40 mM, we would  
 766 only expect a decrease from 100 mM to about 35 mM in the slowest growth conditions. While  
 767 experimental data is limited, amino acid concentrations only decrease to about 60 mM for cells  
 768 grown in minimal media + acetate ( $\lambda \approx 0.3 \text{ hr}^{-1}$  in our proteomic data; value obtained from Bennett  
 769 et al. (2009)), qualitatively consistent with our expectations.

770 Given the quantitative data from Dai et al. (2018), which determined  $f_a$  across the entire range  
 771 of growth rates across our data, we next estimated the active fraction of ribosomal protein. As  
 772 shown in **Figure 11(C)**, we find that cells grow at a rate near the expected translation maximum  
 773 expected from Equation 1, using the maximum elongation rate of  $r_t = 17.1$  aa per second. This is in  
 774 contrast to the reality that ribosomes are translating at almost half this rate in the poorest growth  
 775 conditions. This highlights that there are alternative ways to grow according to the translated-  
 776 limited growth rate that is expected based with ribosomes translating at their maximal elongation  
 777 rate. Specifically, it is by adjusting  $r_t \times R \times f_a$  to match maximal growth rate set by Equation 2, through  
 778 the parameters  $r_{tmax} \times R'$ , that cells are able to maximize their growth rate under steady-state.

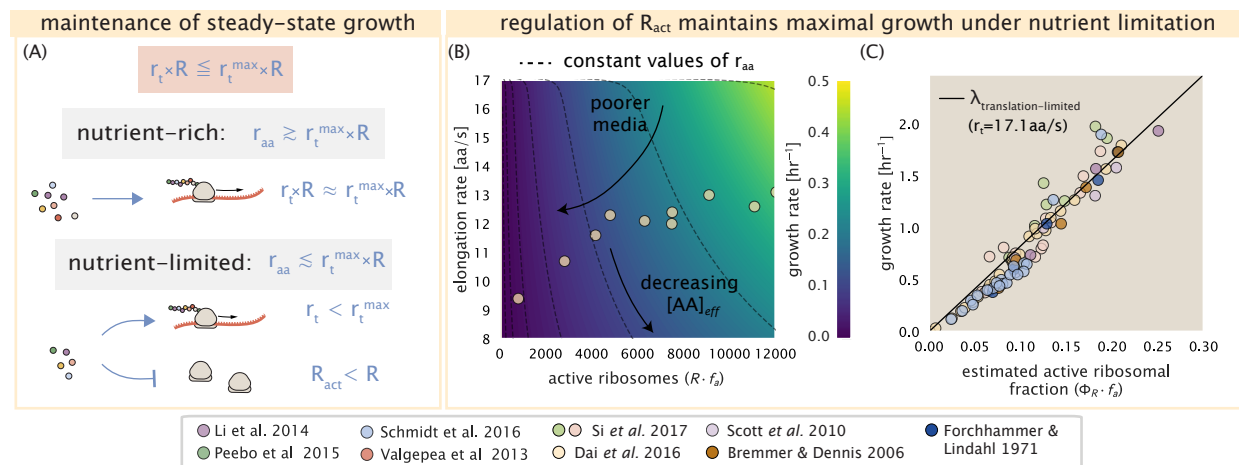


**Figure 11. *E. coli* must regulate ribosomal activity in limiting nutrient conditions.** (A) Schematic showing translation-specific requirements for maintenance of steady-state growth. In a nutrient rich environment, amino acid supply  $r_{aa}$  is sufficiently in excess of the demand by ribosomes translating at their maximal rate. In poorer nutrient conditions, reduced amino acid supply  $r_{aa}$  will decrease the rate of elongation. In a regime where  $r_{aa}$  is less than  $r_t \cdot R$ , the number of actively translating ribosomes will need to be reduced in order to maintain steady-state growth. (B) Translation elongation rate is plotted as a function of the number of actively translating ribosomes  $R \cdot f_a$ . Dashed lines correspond to a range of amino acid synthesis rates  $r_{aa}$ , from  $10^3$  to  $10^6$ . Growth rates are calculated according to Equation 1, assuming a constant ribosomal fraction of 8 percent. See appendix XX for additional details. (C) Experimental data from Dai *et al.* are used to estimate the fraction of actively translating ribosomes. The solid line represents the translation-limited growth rate for ribosomes elongating at 17.1 AA/s.

780 Global regulatory control across central dogma may provide an explanation for the robust scaling laws in *E. coli*.

781 A number of recent papers further highlight the possibility that (p)ppGpp may even provide a causal  
 782 explanation for the scaling laws in *E. coli*. In the context of ribosomal activity, increased levels of  
 783 (p)ppGpp are associated with lower ribosomal content, and at slow growth appear to help reduce the  
 784 fraction of actively translating ribosomes (Dai *et al.*, 2016, 2018). Titration of the cellular (p)ppGpp  
 785 concentrations (up or down) can invoke similar proteomic changes reminiscent of those observed  
 786 under nutrient limitation (Zhu and Dai, 2019). In light of the limiting dependence of ribosome copy  
 787 number on chromosomal gene dosage, it was recently shown that growth in a (p)ppGpp null strain  
 788 abolishes both the scaling in cell size and the  $\langle \# \text{ ori} \rangle / \langle \# \text{ ter} \rangle$  ratio. Instead, cells exhibited a high  
 789  $\langle \# \text{ ori} \rangle / \langle \# \text{ ter} \rangle$  closer to 4 and cell size more consistent with a fast growth state where (p)ppGpp  
 790 levels are low (Fernández-Coll *et al.*, 2020).]

791 [NB, expand on to consider how activity of RNAP and other aspects(?) may follow a similar  
 792 behaviour and are under related control mechanisms.]

## 794      References

- 795      Abelson, H., Johnson, L., Penman, S., and Green, H. (1974). Changes in RNA in relation to growth of the fibroblast:  
 796      II. The lifetime of mRNA, rRNA, and tRNA in resting and growing cells. *Cell*, 1(4):161–165.
- 797      Aidelberg, G., Towbin, B. D., Rothschild, D., Dekel, E., Bren, A., and Alon, U. (2014). Hierarchy of non-glucose  
 798      sugars in *Escherichia coli*. *BMC Systems Biology*, 8(1):133.
- 799      Antonenko, Y. N., Pohl, P., and Denisov, G. A. (1997). Permeation of ammonia across bilayer lipid membranes  
 800      studied by ammonium ion selective microelectrodes. *Biophysical Journal*, 72(5):2187–2195.
- 801      Ashburner, M., Ball, C. A., Blake, J. A., Botstein, D., Butler, H., Cherry, J. M., Davis, A. P., Dolinski, K., Dwight, S. S.,  
 802      Eppig, J. T., Harris, M. A., Hill, D. P., Isbel-Tarver, L., Kasarskis, A., Lewis, S., Matese, J. C., Richardson, J. E.,  
 803      Ringwald, M., Rubin, G. M., and Sherlock, G. (2000). Gene Ontology: tool for the unification of biology. *Nature Genetics*,  
 804      25(1):25–29.
- 805      Ason, B., Bertram, J. G., Hingorani, M. M., Beechem, J. M., O'Donnell, M., Goodman, M. F., and Bloom, L. B.  
 806      (2000). A Model for *Escherichia coli* DNA Polymerase III Holoenzyme Assembly at Primer/Template Ends:  
 807      DNA Triggers A Change In Binding Specificity of the  $\gamma$  Complex Clamp Loader. *Journal of Biological Chemistry*,  
 808      275(4):3006–3015.
- 809      Assentoft, M., Kaptan, S., Schneider, H.-P., Deitmer, J. W., de Groot, B. L., and MacAulay, N. (2016). Aquaporin 4  
 810      as a NH<sub>3</sub> Channel. *Journal of Biological Chemistry*, 291(36):19184–19195.
- 811      Bauer, S. and Ziv, E. (1976). Dense growth of aerobic bacteria in a bench-scale fermentor. *Biotechnology and  
 812      Bioengineering*, 18(1):81–94. \_eprint: <https://onlinelibrary.wiley.com/doi/10.1002/bit.260180107>.
- 813      Belliveau, N. M., Barnes, S. L., Ireland, W. T., Jones, D. L., Sweredoski, M. J., Moradian, A., Hess, S., Kinney, J. B.,  
 814      and Phillips, R. (2018). Systematic approach for dissecting the molecular mechanisms of transcriptional  
 815      regulation in bacteria. *Proceedings of the National Academy of Sciences*, 115(21):E4796–E4805.
- 816      Bennett, B. D., Kimball, E. H., Gao, M., Osterhout, R., Van Dien, S. J., and Rabinowitz, J. D. (2009). Absolute  
 817      metabolite concentrations and implied enzyme active site occupancy in *Escherichia coli*. *Nature Chemical  
 818      Biology*, 5(8):593–599.
- 819      Birnbaum, L. S. and Kaplan, S. (1971). Localization of a Portion of the Ribosomal RNA Genes in *Escherichia coli*.  
 820      *Proceedings of the National Academy of Sciences*, 68(5):925–929.
- 821      Booth, I. R., Mitchell, W. J., and Hamilton, W. A. (1979). Quantitative analysis of proton-linked transport systems.  
 822      The lactose permease of *Escherichia coli*. *Biochemical Journal*, 182(3):687–696.
- 823      Bremer, H. and Dennis, P. P. (2008). Modulation of Chemical Composition and Other Parameters of the Cell at  
 824      Different Exponential Growth Rates. *EcoSal Plus*, 3(1).
- 825      Browning, D. F. and Busby, S. J. W. (2016). Local and global regulation of transcription initiation in bacteria.  
 826      *Nature Reviews Microbiology*, 14(10):638–650.
- 827      Cox, G. B., Newton, N. A., Gibson, F., Snoswell, A. M., and Hamilton, J. A. (1970). The function of ubiquinone in  
 828      *Escherichia coli*. *Biochemical Journal*, 117(3):551–562.
- 829      Dai, X., Zhu, M., Warren, M., Balakrishnan, R., Okano, H., Williamson, J. R., Fredrick, K., and Hwa, T. (2018).  
 830      Slowdown of Translational Elongation in *Escherichia coli* under Hyperosmotic Stress. - PubMed - NCBI. *mBio*,  
 831      9(1):281.
- 832      Dai, X., Zhu, M., Warren, M., Balakrishnan, R., Patsalo, V., Okano, H., Williamson, J. R., Fredrick, K., Wang, Y.-P.,  
 833      and Hwa, T. (2016). Reduction of translating ribosomes enables *Escherichia coli* to maintain elongation rates  
 834      during slow growth. *Nature Microbiology*, 2(2):16231.
- 835      Escalante, A., Salinas Cervantes, A., Gosset, G., and Bolívar, F. (2012). Current knowledge of the *Escherichia coli*  
 836      phosphoenolpyruvate-carbohydrate phosphotransferase system: Peculiarities of regulation and impact on  
 837      growth and product formation. *Applied Microbiology and Biotechnology*, 94(6):1483–1494.
- 838      Feist, A. M., Henry, C. S., Reed, J. L., Krummenacker, M., Joyce, A. R., Karp, P. D., Broadbelt, L. J., Hatzimanikatis,  
 839      V., and Palsson, B. Ø. (2007). A genome-scale metabolic reconstruction for *Escherichia coli* K-12 MG1655 that  
 840      accounts for 1260 ORFs and thermodynamic information. *Molecular Systems Biology*, 3(1):121.

- 841 Fernández-Coll, L., Maciąg-Dorszynska, M., Tailor, K., Vadia, S., Levin, P. A., Szalewska-Palasz, A., Cashel, M.,  
842 and Dunny, G. M. (2020). The Absence of (p)ppGpp Renders Initiation of *Escherichia coli* Chromosomal DNA  
843 Synthesis Independent of Growth Rates. *mBio*, 11(2):45.
- 844 Fijalkowska, I. J., Schaaper, R. M., and Jonczyk, P. (2012). DNA replication fidelity in *Escherichia coli*: A multi-DNA  
845 polymerase affair. *FEMS Microbiology Reviews*, 36(6):1105–1121.
- 846 Finkelstein, I. J. and Greene, E. C. (2013). Molecular Traffic Jams on DNA. *Annual Review of Biophysics*, 42(1):241–  
847 263.
- 848 Gama-Castro, S., Salgado, H., Santos-Zavaleta, A., Ledezma-Tejeida, D., Muñiz-Rascado, L., García-Sotelo, J. S.,  
849 Alquicira-Hernández, K., Martínez-Flores, I., Pannier, L., Castro-Mondragón, J. A., Medina-Rivera, A., Solano-  
850 Lira, H., Bonavides-Martínez, C., Pérez-Rueda, E., Alquicira-Hernández, S., Porrón-Sotelo, L., López-Fuentes,  
851 A., Hernández-Koutoucheva, A., Moral-Chávez, V. D., Rinaldi, F., and Collado-Vides, J. (2016). RegulonDB  
852 version 9.0: High-level integration of gene regulation, coexpression, motif clustering and beyond. *Nucleic  
853 Acids Research*, 44(D1):D133–D143.
- 854 Ge, J., Yu, G., Ator, M. A., and Stubbe, J. (2003). Pre-Steady-State and Steady-State Kinetic Analysis of *E. coli* Class  
855 I Ribonucleotide Reductase. *Biochemistry*, 42(34):10071–10083.
- 856 Godin, M., Delgado, F. F., Son, S., Grover, W. H., Bryan, A. K., Tzur, A., Jorgensen, P., Payer, K., Grossman, A. D.,  
857 Kirschner, M. W., and Manalis, S. R. (2010). Using buoyant mass to measure the growth of single cells. *Nature  
858 Methods*, 7(5):387–390.
- 859 Goldman, S. R., Nair, N. U., Wells, C. D., Nickels, B. E., and Hochschild, A. (2015). The primary  $\sigma$  factor in *Es-  
860 cherichia coli* can access the transcription elongation complex from solution *in vivo*. *eLife*, 4:e10514.
- 861 Harris, L. K. and Theriot, J. A. (2018). Surface Area to Volume Ratio: A Natural Variable for Bacterial Morphogen-  
862 esis. *Trends in microbiology*, 26(10):815–832.
- 863 Harris, R. M., Webb, D. C., Howitt, S. M., and Cox, G. B. (2001). Characterization of PitA and PitB from *Escherichia  
864 coli*. *Journal of Bacteriology*, 183(17):5008–5014.
- 865 Heldal, M., Norland, S., and Tumyr, O. (1985). X-ray microanalytic method for measurement of dry matter and  
866 elemental content of individual bacteria. *Applied and Environmental Microbiology*, 50(5):1251–1257.
- 867 Henkel, S. G., Beek, A. T., Steinsiek, S., Stagge, S., Bettenbrock, K., de Mattos, M. J. T., Sauter, T., Sawodny, O.,  
868 and Ederer, M. (2014). Basic Regulatory Principles of *Escherichia coli*'s Electron Transport Chain for Varying  
869 Oxygen Conditions. *PLoS ONE*, 9(9):e107640.
- 870 Hui, S., Silverman, J. M., Chen, S. S., Erickson, D. W., Basan, M., Wang, J., Hwa, T., and Williamson, J. R. (2015).  
871 Quantitative proteomic analysis reveals a simple strategy of global resource allocation in bacteria. *Molecular  
872 Systems Biology*, 11(2):e784–e784.
- 873 Ingledew, W. J. and Poole, R. K. (1984). The respiratory chains of *Escherichia coli*. *Microbiological Reviews*,  
874 48(3):222–271.
- 875 Ireland, W. T., Beeler, S. M., Flores-Bautista, E., Belliveau, N. M., Sweredoski, M. J., Moradian, A., Kinney, J. B.,  
876 and Phillips, R. (2020). Deciphering the regulatory genome of *Escherichia coli*, one hundred promoters at a  
877 time. *bioRxiv*.
- 878 Jacob, F. and Monod, J. (1961). Genetic regulatory mechanisms in the synthesis of proteins. *Journal of Molecular  
879 Biology*, 3(3):318–356.
- 880 Jensen, R. B., Wang, S. C., and Shapiro, L. (2001). A moving DNA replication factory in *Caulobacter crescentus*.  
881 *The EMBO journal*, 20(17):4952–4963.
- 882 Jun, S., Si, F., Pugatch, R., and Scott, M. (2018). Fundamental principles in bacterial physiology - history, recent  
883 progress, and the future with focus on cell size control: A review. *Reports on Progress in Physics*, 81(5):056601.
- 884 Kapanidis, A. N., Margeat, E., Laurence, T. A., Doose, S., Ho, S. O., Mukhopadhyay, J., Kortkhonjia, E., Mekler, V.,  
885 Ebright, R. H., and Weiss, S. (2005). Retention of Transcription Initiation Factor  $\Sigma$ 70 in Transcription Elonga-  
886 tion: Single-Molecule Analysis. *Molecular Cell*, 20(3):347–356.
- 887 Khademi, S., O'Connell, J., Remis, J., Robles-Colmenares, Y., Miercke, L.J.W., and Stroud, R. M. (2004). Mechanism  
888 of Ammonia Transport by Amt/MEP/Rh: Structure of AmtB at 1.35 Å. *Science*, 305(5690):1587–1594.

- 889 Khademian, M. and Imlay, J. A. (2017). *Escherichia coli* cytochrome c peroxidase is a respiratory oxidase that  
890 enables the use of hydrogen peroxide as a terminal electron acceptor. *Proceedings of the National Academy  
891 of Sciences*, 114(33):E6922–E6931.
- 892 Li, G.-W., Burkhardt, D., Gross, C., and Weissman, J. S. (2014). Quantifying absolute protein synthesis rates  
893 reveals principles underlying allocation of cellular resources. *Cell*, 157(3):624–635.
- 894 Liebermeister, W., Noor, E., Flamholz, A., Davidi, D., Bernhardt, J., and Milo, R. (2014). Visual account of protein  
895 investment in cellular functions. *Proceedings of the National Academy of Sciences*, 111(23):8488–8493.
- 896 Liu, M., Durfee, T., Cabrera, J. E., Zhao, K., Jin, D. J., and Blattner, F. R. (2005). Global Transcriptional Programs  
897 Reveal a Carbon Source Foraging Strategy by *Escherichia coli*. *Journal of Biological Chemistry*, 280(16):15921–  
898 15927.
- 899 Lynch, M. and Marinov, G. K. (2015). The bioenergetic costs of a gene. *Proceedings of the National Academy of  
900 Sciences*, 112(51):15690–15695.
- 901 Maaløe, O. (1979). *Regulation of the Protein-Synthesizing Machinery—Ribosomes, tRNA, Factors, and So On*. Gene  
902 Expression. Springer.
- 903 Milo, R., Jorgensen, P., Moran, U., Weber, G., and Springer, M. (2010). BioNumbers—the database of key num-  
904 bers in molecular and cell biology. *Nucleic Acids Research*, 38(suppl\_1):D750–D753.
- 905 Monod, J. (1947). The phenomenon of enzymatic adaptation and its bearings on problems of genetics and  
906 cellular differentiation. *Growth Symposium*, 9:223–289.
- 907 Mooney, R. A., Darst, S. A., and Landick, R. (2005). Sigma and RNA Polymerase: An On-Again, Off-Again Rela-  
908 tionship? *Molecular Cell*, 20(3):335–345.
- 909 Mooney, R. A. and Landick, R. (2003). Tethering  $\Sigma$ 70 to RNA polymerase reveals high *in vivo* activity of  $\sigma$  factors  
910 and  $\Sigma$ 70-dependent pausing at promoter-distal locations. *Genes & Development*, 17(22):2839–2851.
- 911 Neidhardt, F. C., Ingraham, J., and Schaechter, M. (1991). *Physiology of the Bacterial Cell - A Molecular Approach*,  
912 volume 1. Elsevier.
- 913 Ojkic, N., Serbanescu, D., and Banerjee, S. (2019). Surface-to-volume scaling and aspect ratio preservation in  
914 rod-shaped bacteria. *eLife*, 8:642.
- 915 Patrick, M., Dennis, P. P., Ehrenberg, M., and Bremer, H. (2015). Free RNA polymerase in *Escherichia coli*.  
916 *Biochimie*, 119:80–91.
- 917 Peebo, K., Valgepea, K., Maser, A., Nahku, R., Adamberg, K., and Vilu, R. (2015). Proteome reallocation in *Es-  
918 cherichia coli* with increasing specific growth rate. *Molecular BioSystems*, 11(4):1184–1193.
- 919 Perdue, S. A. and Roberts, J. W. (2011).  $\sigma^{70}$ -dependent Transcription Pausing in *Escherichia coli*. *Journal of  
920 Molecular Biology*, 412(5):782–792.
- 921 Phillips, R. (2018). Membranes by the Numbers. In *Physics of Biological Membranes*, pages 73–105. Springer,  
922 Cham, Cham.
- 923 Ramos, S. and Kaback, H. R. (1977). The relation between the electrochemical proton gradient and active trans-  
924 port in *Escherichia coli* membrane vesicles. *Biochemistry*, 16(5):854–859.
- 925 Rosenberg, H., Gerdes, R. G., and Chegwidden, K. (1977). Two systems for the uptake of phosphate in *Escherichia  
926 coli*. *Journal of Bacteriology*, 131(2):505–511.
- 927 Rudd, S. G., Valerie, N. C. K., and Helleday, T. (2016). Pathways controlling dNTP pools to maintain genome  
928 stability. *DNA Repair*, 44:193–204.
- 929 Sánchez-Romero, M. A., Molina, F., and Jiménez-Sánchez, A. (2011). Organization of ribonucleoside diphosphate  
930 reductase during multifork chromosome replication in *Escherichia coli*. *Microbiology*, 157(8):2220–2225.
- 931 Schaechter, M., Maaløe, O., and Kjeldgaard, N. O. (1958). Dependency on Medium and Temperature of Cell Size  
932 and Chemical Composition during Balanced Growth of *Salmonella typhimurium*. *Microbiology*, 19(3):592–606.
- 933 Schmidt, A., Kochanowski, K., Vedelaar, S., Ahrné, E., Volkmer, B., Callipo, L., Knoops, K., Bauer, M., Aebersold,  
934 R., and Heinemann, M. (2016). The quantitative and condition-dependent *Escherichia coli* proteome. *Nature  
935 Biotechnology*, 34(1):104–110.

- 936 Scholz, S. A., Diao, R., Wolfe, M. B., Fivenson, E. M., Lin, X. N., and Freddolino, P. L. (2019). High-Resolution  
 937 Mapping of the *Escherichia coli* Chromosome Reveals Positions of High and Low Transcription. *Cell Systems*,  
 938 8(3):212–225.e9.
- 939 Scott, M., Gunderson, C. W., Mateescu, E. M., Zhang, Z., and Hwa, T. (2010). Interdependence of cell growth and  
 940 gene expression: origins and consequences. *Science*, 330(6007):1099–1102.
- 941 Sekowska, A., Kung, H.-F., and Danchin, A. (2000). Sulfur Metabolism in *Escherichia coli* and Related Bacteria:  
 942 Facts and Fiction. *Journal of Molecular Microbiology and Biotechnology*, 2(2):34.
- 943 Si, F., Le Treut, G., Sauls, J. T., Vadia, S., Levin, P. A., and Jun, S. (2019). Mechanistic Origin of Cell-Size Control  
 944 and Homeostasis in Bacteria. *Current Biology*, 29(11):1760–1770.e7.
- 945 Si, F., Li, D., Cox, S. E., Sauls, J. T., Azizi, O., Sou, C., Schwartz, A. B., Erickstad, M. J., Jun, Y., Li, X., and Jun, S. (2017).  
 946 Invariance of Initiation Mass and Predictability of Cell Size in *Escherichia coli*. *Current Biology*, 27(9):1278–1287.
- 947 Sirko, A., Zatyka, M., Sadowy, E., and Hulanicka, D. (1995). Sulfate and thiosulfate transport in *Escherichia coli* K-  
 948 12: Evidence for a functional overlapping of sulfate- and thiosulfate-binding proteins. *Journal of Bacteriology*,  
 949 177(14):4134–4136.
- 950 Stasi, R., Neves, H. I., and Spira, B. (2019). Phosphate uptake by the phosphonate transport system PhnCDE.  
 951 *BMC Microbiology*, 19.
- 952 Stevenson, B. S. and Schmidt, T. M. (2004). Life History Implications of rRNA Gene Copy Number in *Escherichia*  
 953 *coli*. *Applied and Environmental Microbiology*, 70(11):6670–6677.
- 954 Stouthamer, A. H. (1973). A theoretical study on the amount of ATP required for synthesis of microbial cell  
 955 material. *Antonie van Leeuwenhoek*, 39(1):545–565.
- 956 Stouthamer, A. H. and Bettenhausen, C. W. (1977). A continuous culture study of an ATPase-negative mutant  
 957 of *Escherichia coli*. *Archives of Microbiology*, 113(3):185–189.
- 958 Svenningsen, S. L., Kongstad, M., Stenum, T. S. n., Muñoz-Gómez, A. J., and Sørensen, M. A. (2017). Transfer RNA  
 959 is highly unstable during early amino acid starvation in *Escherichia coli*. *Nucleic Acids Research*, 45(2):793–804.
- 960 Szenk, M., Dill, K. A., and de Graff, A. M. R. (2017). Why Do Fast-Growing Bacteria Enter Overflow Metabolism?  
 961 Testing the Membrane Real Estate Hypothesis. *Cell Systems*, 5(2):95–104.
- 962 Taheri-Araghi, S., Bradde, S., Sauls, J. T., Hill, N. S., Levin, P. A., Paulsson, J., Vergassola, M., and Jun, S. (2015).  
 963 Cell-size control and homeostasis in bacteria. - PubMed - NCBI. *Current Biology*, 25(3):385–391.
- 964 Tatusov, R. L., Galperin, M. Y., Natale, D. A., and Koonin, E. V. (2000). The COG database: a tool for genome-scale  
 965 analysis of protein functions and evolution. *Nucleic Acids Research*, 28(1):33–36.
- 966 Taymaz-Nikerel, H., Borujeni, A. E., Verheijen, P. J. T., Heijnen, J. J., and van Gulik, W. M. (2010).  
 967 Genome-derived minimal metabolic models for *Escherichia coli* mg1655 with estimated in vivo  
 968 respiratory ATP stoichiometry. *Biotechnology and Bioengineering*, 107(2):369–381. \_eprint:  
 969 <https://onlinelibrary.wiley.com/doi/pdf/10.1002/bit.22802>.
- 970 The Gene Ontology Consortium (2018). The Gene Ontology Resource: 20 years and still GOing strong. *Nucleic  
 971 Acids Research*, 47(D1):D330–D338.
- 972 Valgepea, K., Adamberg, K., Seiman, A., and Vilu, R. (2013). *Escherichia coli* achieves faster growth by increasing  
 973 catalytic and translation rates of proteins. *Molecular BioSystems*, 9(9):2344.
- 974 van Heeswijk, W. C., Westerhoff, H. V., and Boogerd, F. C. (2013). Nitrogen Assimilation in *Escherichia coli*: Putting  
 975 Molecular Data into a Systems Perspective. *Microbiology and Molecular Biology Reviews*, 77(4):628–695.
- 976 Weber, J. and Senior, A. E. (2003). ATP synthesis driven by proton transport in F1FO-ATP synthase. *FEBS Letters*,  
 977 545(1):61–70.
- 978 Willsky, G. R., Bennett, R. L., and Malamy, M. H. (1973). Inorganic Phosphate Transport in *Escherichia coli*: Involvement  
 979 of Two Genes Which Play a Role in Alkaline Phosphatase Regulation. *Journal of Bacteriology*, 113(2):529–  
 980 539.
- 981 Zhang, L., Jiang, W., Nan, J., Almqvist, J., and Huang, Y. (2014a). The *Escherichia coli* CysZ is a pH dependent sulfate  
 982 transporter that can be inhibited by sulfite. *Biochimica et Biophysica Acta (BBA) - Biomembranes*, 1838(7):1809–  
 983 1816.

- 984 Zhang, Z., Aboulwafa, M., and Saier, M. H. (2014b). Regulation of crp gene expression by the catabolite repres-  
985 sor/activator, cra, in *Escherichia coli*. *Journal of Molecular Microbiology and Biotechnology*, 24(3):135–141.
- 986 Zhu, M. and Dai, X. (2019). Growth suppression by altered (p)ppGpp levels results from non-optimal resource  
987 allocation in *Escherichia coli*. *Nucleic Acids Research*, 47(9):4684–4693.